EBioMedicine 31 (2018) 202–216

Contents lists available at ScienceDirect

EBioMedicine

journal homepage: www.ebiomedicine.com

Research Paper

Adipocyte-derived Lysophosphatidylcholine Activates Adipocyte and Adipose Tissue Macrophage Nod-Like Receptor Protein 3 Inflammasomes Mediating Homocysteine-Induced Insulin Resistance

Song-Yang Zhang [a,1], Yong-Qiang Dong [a,1], Pengcheng Wang [a], Xingzhong Zhang [a], Yu Yan [a], Lulu Sun [a], Bo Liu [a], Dafang Zhang [b], Heng Zhang [c], Huiying Liu [a], Wei Kong [a], Gang Hu [d,e], Yatrik M. Shah [f], Frank J. Gonzalez [g], Xian Wang [a,*], Changtao Jiang [a,*]

[a] Department of Physiology and Pathophysiology, School of Basic Medical Sciences, Peking University, Key Laboratory of Molecular Cardiovascular Science, Ministry of Education, Beijing 100191, People's Republic of China
[b] Department of Hepatobiliary Surgery, Peking University People's Hospital, Peking University, Beijing 100044, People's Republic of China
[c] Department of Endocrinology, Beijing Chao-Yang Hospital, Capital Medical University, Beijing 100020, People's Republic of China
[d] Department of Pharmacology, School of Basic Medical Sciences, Nanjing Medical University, Jiangsu Key Laboratory of Neurodegeneration, Nanjing 210029, Jiangsu, People's Republic of China
[e] Department of Pharmacology, School of Basic Medical Sciences, Nanjing University of Chinese Medicine, Nanjing 210023, Jiangsu, People's Republic of China
[f] Department of Molecular & Integrative Physiology, Division of Gastroenterology, University of Michigan Medical School, Ann Arbor, MI, USA
[g] Center for Cancer Research, National Cancer Institute, National Institutes of Health, Bethesda, MD, USA

ARTICLE INFO

Article history:
Received 9 March 2018
Received in revised form 5 April 2018
Accepted 23 April 2018
Available online 27 April 2018

Keywords:
Insulin resistance
NLRP3 inflammasome
Homocysteine
Adipocyte
Adipose tissue macrophage

ABSTRACT

The adipose Nod-like receptor protein 3 (NLRP3) inflammasome senses danger-associated molecular patterns (DAMPs) and initiates insulin resistance, but the mechanisms of adipose inflammasome activation remains elusive. In this study, Homocysteine (Hcy) is revealed to be a DAMP that activates adipocyte NLRP3 inflammasomes, participating in insulin resistance. Hcy-induced activation of NLRP3 inflammasomes were observed in both adipocytes and adipose tissue macrophages (ATMs) and mediated insulin resistance. Lysophosphatidylcholine (lyso-PC) acted as a second signal activator, mediating Hcy-induced adipocyte NLRP3 inflammasome activation. Hcy elevated adipocyte lyso-PC generation in a hypoxia-inducible factor 1 (HIF1)-phospholipase A2 group 16 (PLA2G16) axis-dependent manner. Lyso-PC derived from the Hcy-induced adipocyte also activated ATM NLRP3 inflammasomes in a paracrine manner. This study demonstrated that Hcy activates adipose NLRP3 inflammasomes in an adipocyte lyso-PC-dependent manner and highlights the importance of the adipocyte NLRP3 inflammasome in insulin resistance.

1. Introduction

Chronic inflammation, characterized by increased macrophage infiltration, is a common feature of adipose insulin resistance. The activated adipocytes and adipose tissue macrophages (ATMs) coordinately promote insulin resistance by increasing pro-inflammatory cytokines secretion [1,2], immune cells activation [3,4] and exosomes release [5,6]. Activation of adipocytes and ATMs relies on the pattern-recognition receptors (PRRs) to sense various pathogen-associated molecular patterns (PAMPs) or danger-associated molecular patterns (DAMPs) [7,8]. Inflammasomes are a class of intracellular PRRs [9]. Once activated, inflammasome recruits Caspase1 (CASP1), and triggers its self-processing [10]. Processed CASP1 cleavages a number of cytokines, including interleukin (IL) 1β and IL18, participating in the onset of infectious diseases [11], autoimmune diseases [12] and cardiometabolic diseases [13,14]. Among the various types of inflammasomes, the nod-like receptor protein 3 (NLRP3) inflammasome has been extensively studied in adipose tissue. The *Nlrp3*, *Casp1* and *Il1b* knockout mice were protected from high-fat diet-induced adipose insulin resistance [15–18], but it is unclear if activation of the adipose NLRP3 inflammasome depends on adipocytes or ATMs. Some studies reported that the inflammasome components were highly expressed in the ATMs and co-localized only with ATM marker [17]. However, other studies proved the expression of inflammasome components in mouse and human primary adipocytes [19,20]. Activation of the adipocyte inflammasome was involved in adipogenesis and the depletion of macrophages did not affect the inflammasome activation in adipose tissue [15].

* Corresponding authors at: Department of Physiology and Pathophysiology, School of Basic Medical Sciences, Peking University, Beijing 100191, People's Republic of China.
E-mail addresses: xwang@bjmu.edu.cn, (X. Wang), jiangchangtao@bjmu.edu.cn (C. Jiang).
[1] These authors contributed equally.

https://doi.org/10.1016/j.ebiom.2018.04.022

Homocysteine (Hcy) is a sulfur-containing non-proteinogenic amino acid, involved in the methionine cycle. An increased plasma Hcy level (>15 μM), is an independent risk factor of cardiovascular disease and is clinically defined as hyperhomocysteinemia (HHcy) [21–23]. Apart from the cardiovascular effect of Hcy, a series of clinical studies have also revealed a closely association between HHcy and insulin resistance. Patients with insulin resistance and type II diabetes mellitus display increased plasma levels of Hcy [24–26]. A methylenetetrahydrofolate reductase C677T polymorphism that interferes with the methionine cycle and elevates plasma Hcy levels, is positively associated with insulin resistance [27,28]. Folic acid administration, in contrast, lowers the plasma level of Hcy and improves insulin sensitivity in obese children [29]. Our previous studies have established an HHcy mouse model by treating mice with Hcy in drinking water. The Hcy-treated mice mimic clinical HHcy patients well and exhibited an increased atherosclerosis [30]. The plasma levels of Hcy are positively associated with abdominal adiposity in humans [26]. In the mouse model of HHcy, Hcy was found to be enriched in adipose tissue, promoting insulin resistance and adipose inflammation [31,32], but the exact mechanisms is still elusive.

Our previous study has revealed that the activation of NLRP3 inflammasome aggravates Hcy-induced abdominal aortic aneurysm [33], but whether NLRP3 inflammasome is also involved in the Hcy-induced insulin resistance is unknown. In this study, Hcy-induced activation of the adipocyte and ATM NLRP3 inflammasomes was observed in adipose tissue and mediated insulin resistance. Hcy acted as a second signal activator of the adipocyte NLRP3 inflammasome, which was mediated by lysophosphatidylcholine (lyso-PC) through the adipocyte hypoxia-inducible factor 1 (HIF1)-phospholipase A2 group 16 (PLA2G16) axis. Finally, lyso-PC derived from the Hcy-treated adipocytes activated ATM NLRP3 inflammasomes in a paracrine manner.

2. Materials and Methods

2.1. Subject Sample Collection

The subject plasma samples were collected under a study approved by the Ethics Committee of Beijing Chao-Yang Hospital [34]. The blood samples from all subjects were placed in tubes containing EDTA and aprotinin (500 kIU/ml), and centrifuged immediately, then stored at −80 °C. The subject adipose tissue samples were collected under a study approved by the Ethics Committee of Peking University People's Hospital. The subject adipose tissue (3–5 g per subject) was excised from the omental adipose tissue of metabolically healthy subjects, undergoing abdominal surgery. The pre-adipocytes were isolated and differentiated to adipocytes, which was described in detail in the cell culture section. The studies complied with the Code of Ethics of the World Medical Association (Declaration of Helsinki). All subjects provided written informed consent prior to participation.

2.2. Animals and Housing

All mice were housed under specific pathogen free condition in a temperature-controlled room (22 °C) with a 12 h light and dark cycle and were given free access to a normal chow diet (Cat. 1025, HFK Biosciences, Beijing, China) and drinking water. Wild type (WT) mice were C57BL/6 J background and were obtained from Vital River Laboratories (Beijing, China). The Casp1 knockout (*Casp1*$^{-/-}$) and corresponding WT mice were obtained from Jackson Laboratory (Cat. 004947, Bar Harbor, ME, USA, RRID: MGI_3574069) [35] and were backcrossed to the C57BL/6 J background after 10 generations. The adipocyte-specific *Hif1a* knockout (*Hif1a*$^{\Delta Ad}$), adipocyte-specific *Hif1a* transgenic (*Hif1a*^{LSL}) and corresponding WT mice were on the C57BL/6 J background and were generated using the Cre-loxP system. The *Hif1a* flox (*Hif1a*$^{fl/fl}$) mice (RRID: MGI_3815313) were published previously [36]. *Hif1a*^{LSL} mice were described in an earlier study [37,38]. To exclude the confounding effect of aP2-Cre in macrophages, the adiponectin-Cre mice was used to generate *Hif1a*$^{\Delta Ad}$ and *Hif1a*^{LSL} mice, which was obtained from Jackson Laboratory (Cat. 028020, Bar Harbor, ME, USA, RRID: IMSR_JAX: 024671) [39]. All animal protocols were approved by the Animal Care and Use Committee of Peking University.

2.3. HHcy Mouse Models

The HHcy mouse model has been reported previously [31]. In brief, male 6- to 8-week-old mice were fed drinking water containing DL-Hcy (1.8 g/l) or not for the indicated periods. The drinking water was loaded in a bottle protected from light and changed every day. The DL-Hcy was purchased from Sigma-Aldrich Chemicals (Cat. H4628, St. Louis, MO, USA).

2.4. Glucose Tolerance Test and Insulin Tolerance Test

For the glucose tolerance test (GTT), mice were fasted for 12 h before the administration of glucose (1.8 g/kg, i. p.). Blood samples were drawn from a cut at the tip of the tail at 0, 30, 60, 90 and 120 min after glucose administration, and blood glucose concentrations were measured immediately. For insulin tolerance test (ITT), mice were fasted for 4 h before the administration of insulin (1 IU/kg, i. p.). Blood samples were drawn from a cut at the tip of the tail at 0, 30, 60, 90 and 120 min after insulin administration, and blood glucose concentrations were measured immediately.

2.5. Bone Marrow Transplantation

Prior to bone marrow transplantation (BMT), 8-week-old recipient mice were provided antibiotic drinking water containing neomycin (100 mg/l) and polymyxin B sulfate (10 mg/l) for 1 week and were lethally irradiated (9 Gy, Co^{60} source). Four hours later, the recipient mice were transplanted with bone marrow (5×10^6 mononuclear cells per mouse) *via* tail vein injection. The bone marrow was isolated from the femurs of 2- to 4-week old donor mice. The recipient mice were maintained on antibiotic water for another 2 weeks. Six weeks after the transplantation, recipient mice were used for experiments.

2.6. Cytometric Bead Array and FLICA-CASP1 Assay

The inflammatory cytokine levels in plasma were investigated using a cytometric bead array mouse inflammation kit (Cat. 552364, BD Biosciences, San Jose, CA, USA), according to the manufacturer's instructions.

For fluorescent labeled inhibitors of CASP assay (FLICA)-CASP1 assay, the flowcytometry (FCM) analysis of adipocytes and SVF cells were conducted according to the previous studies [40,41]. In brief, epididymal white adipose tissue (eWAT) was minced and digested by type I collagenase (0.8 mg/ml) for 20–30 min. Primary adipocytes and stromal vascular fraction (SVF) cells were separated and stained with FAM-YVAD-FMK (Cat. 98, ImmunoChemistry Technologies, Bloomington, MN, USA) for 2 h, according to the manufacturer's instructions. The stained cells were analyzed using a BD FACS Calibur with Cell QuestPro software (BD Biosciences, San Jose, CA, USA).

2.7. Cell Culture

The 3T3-L1 cell line (Cat. 3111C0001CCC000155) and 293T cell line (Cat. 3111C0002000000112) were purchased from the Cell Resource Center of China (Beijing, China). The 3T3-L1 and 293T cells were cultured in DMEM-high glucose plus 10% fetal bovine serum (FBS). For the differentiation of 3T3-L1 cells, the cells were cultured for another 2 days after achieving confluent and were treated with insulin

(5 μg/ml), IBMX (500 μM) and dexamethasone (0.1 μM) for 2 days. Then, the medium was changed every 2 days twice.

Mature rat primary adipocytes were isolated from eWAT of Sprague-Dawley (SD) rats (160 to 200 g). The eWAT was minced and incubated at 37 °C for 25 min in type I collagenase (0.8 mg/ml). The packed adipocytes were washed by DMEM-low glucose for 3 times and diluted in DMEM-low glucose to generate a 10% (vol/vol) cell suspension.

The subject adipose tissue was minced into pieces and incubated at 37 °C for 1 h in type I collagenase (0.8 mg/ml). The fluid was centrifuged at 500 *g* for 5 min and suspended by DMEM-F12 medium plus 10% FBS. Twenty four hours later, the cells were changed with fresh medium and treated with insulin (5 μg/ml), dexamethasone (0.1 μM), IBMX (500 μM), indomethacin (60 μM) and biotin (33 μM) for 2 days. Then, the cells were changed with fresh medium and treated with insulin (5 μg/ml) and biotin (33 μM) for another 2 days. The medium was changed every 2 days twice.

For mouse primary peritoneal macrophages, thioglycollate medium (2 ml per mouse, i. p.) was injected to mice. Three days later, the mice were sacrificed and injected with PBS plus 10% FBS (10 ml per mouse, i. p.). The fluid was aspirated from the peritoneum and centrifuged at 400 g for 10 min. The cells were suspended by RPMI-1640 medium plus 10% FBS. The medium was changed 3 h later.

2.8. Materials for Cell Experiments

Lipopolysaccharides (LPS) was purchased from Sigma-Aldrich Chemicals (Cat. L2630, St. Louis, MO, USA). Glyburide was purchased from Aladdin (Cat. G127198, Shanghai, China). Lyso-PC (16:0) was purchased from Avanti Polar Lipids (Cat. 855675, Alabaster, AL, USA). Acriflavine (ACF) was purchased from MCE (Cat. HY-100575, Monmouth Junction, NJ, USA).

2.9. CASP1 Activity Determination

The activity of CASP1 was measured using CASP1 Colorimetric Assay Kit (Cat. K111, BioVision, San Francisco, CA, USA) according to the manufacturer's instructions.

2.10. Plasmid, siRNA and Cell Transfection

The *Pla2g16* mRNA-specific siRNA (si-PLA2G16) and scramble siRNA (si-Scramble) (Cat. siN05815122147-1-5) siRNA were synthesized by RiboBio (Guangzhou, Guangdong, China). The sequence of si-PLA2G16 was listed in Table S1. Oxygen-stable mouse *Hif1a* and the corresponding vector plasmids were published previously [42]. Murine *Pla2g16* promoter, containing the hypoxia response element (HRE), was synthesized and inserted into the pGL3-basic luciferase reporter vector (Cat. U47295, Promega, Madison, WI, USA). The cells were transfected by HiGene (Cat. C1507, Applygen, Beijing, China), according to the manufacturer's instructions.

2.11. Chromatin Immunoprecipitation

The chromatin immunoprecipitation (ChIP) for adipocytes was performed as described previously [43]. In brief, the cells were fixed in formaldehyde to cross-link chromatin, followed by quenching with glycine. The cells were collected by ChIP lysis buffer, and the chromatin DNA was sheared to fragments (approximately 100–300 bp) using the M220 Focused-ultrasonicator (Covaris, Woburn, MA, USA). The samples were incubated with anti-HIF1α (Cat. sc-10790, Santa Cruz Biotechnology, Dallas, TX, USA, RRID: AB_2116990) or anti-IgG (Cat. sc-2027, Santa Cruz Biotechnology, Dallas, TX, USA, RRID: AB_737197) antibody (2 μg) in the ChIP lysis buffer containing bovine serum albumin (BSA) (1 μg/ml). Protein A/G plus-agarose beads (Cat. sc-2003, Santa Cruz Biotechnology, Dallas, TX, USA) were prepared and added to the samples, incubating overnight at 4 °C. The beads were washed with ChIP wash buffer 1 to 4. The DNA fragments were eluted by ChIP elution buffer and were purified by phenol-chloroform-isoamyl alcohol, then were precipitated with glycogen, NaAc (pH = 4.5) and ethanol overnight. The DNA fragments were suspended in ultrapure water and were quantitated by quantitative PCR (qPCR) analysis. The primer sequences were listed in Table S2.

2.12. Luciferase Reporter Assay

The 293T cells were co-transfected with the *Pla2g16* promoter reporter plasmid, phRL-TK Renilla luciferase control plasmid and the oxygen-stable murine HIF1α or corresponding vector plasmid for 24 h. The luciferase assay was performed with the Dual-Luciferase Reporter Assay System (Cat. E1910, Promega, Madison, WI, USA), according to the manufacturer's instructions.

2.13. Lipidomics Analysis

The sample preparation and the lipidomics analysis were undertaken as described previously [44]. In brief, eWAT or cells (20 mg) were homogenized with ultrapure water (200 μl) and then extracted with chloroform-methanol (2:1) solution (1000 μl). The samples were incubated at 37 °C for 30 min and subsequently centrifuged at 16,000 *g* for 20 min at 4 °C. The lower organic phase (approximately 500 μl) was collected and evaporated. The organic residue was dissolved in isopropanol-acetonitrile (1:1) solution (100 μl). Samples were analyzed by the Thermo Scientific Dionex UltiMate 3000 Rapid Separation LC system (Thermo Fisher Scientific, Waltham, MA, USA). Peak extraction and integration were operated with Xcalibur 2.2 SP1.48 software (Thermo Fisher Scientific, Waltham, MA, USA).

2.14. PLA2 Activity Determination

The activity of PLA2 was measured using Phospholipase A2 Assay Kit (Cat. E10217, Thermo Fisher Scientific, Waltham, MA, USA), according to the manufacturer's instructions.

2.15. ELISA

The levels of IL1β and TNFα in plasma and supernatant were measured using IL1β ELISA Kit (Cat. EM001 for murine and Cat. EH001 for human) and TNFα ELISA kit (Cat. EM008), according to the manufacturer's instructions. The ELISA kits were all purchased from ExCell Bio (Shanghai, China).

2.16. Western Blot

Total protein was isolated with RIPA lysis buffer (Cat. P0013C, Beyotime Biotechnology, Shanghai, China). Total protein was subjected to sodium dodecyl sulfate polyacrylamide gel electrophoresis on a 10% or 12% running gel and then transferred to a polyvinylidene fluoride membrane. The membrane was incubated with 10% BSA in Tris Tween-buffered saline at room temperature for 1 h, with different primary antibodies at 4 °C for 12 h and with a horseradish peroxidase (HRP)-conjugated secondary antibody for 1.5 h. The bands were detected with ChemiDOC XRS System (Bio-Rad, Hercules, CA, USA). The full western blot was presented in the supplementary materials. Anti-CASP1 (Cat. sc-56036, RRID: AB_781816) and anti-PLA2G16 (Cat. sc-168105, RRID: AB_10840370) antibodies were purchased from Santa Cruz Biotechnology (Dallas, TX, USA). Anti-IL1β (Cat. AF-401-NA, RRID: AB_416684) antibody was purchased from R&D Systems (Minneapolis, MN, USA). Anti-HIF1α (Cat. 2090-1-AP, RRID: AB_10732601) antibody was purchased from Proteintech Group (Rosemont, IL, USA). Anti-β-actin (Cat. 8457, RRID: AB_10950489) antibody was purchased from Cell Signaling Technology (Danvers, MA, USA). The HRP-conjugated anti-rabbit IgG (Cat. sc-2004, RRID: AB_631746), HRP-conjugated anti-goat IgG (Cat. sc-2020, RRID:

AB_631728) and HRP-conjugated anti-mouse IgG (Cat. sc-2005, RRID: AB_631736) secondary antibodies were all purchased from Santa Cruz Biotechnology (Dallas, TX, USA).

2.17. Quantitative PCR Measurement of mRNA Levels

Total RNA was isolated using TRIzol Reagent (Cat. 15596018, Thermo Fisher Scientific, Waltham, MA, USA). Total RNA (2 μg) was reverse transcribed using 5X All-In-One RT MasterMix (Cat. G490, abm, Richmond, BC, Canada). The quantitative PCR (qPCR) analysis was performed with RealStar Green Power Mixture (Cat. A314, GenStar, Beijing, China) and ran on Mx3000 Multiplex Quantitative PCR System (Agilent, La Jolla, CA, USA). The amount of the PCR products formed in each cycle was evaluated by the fluorescence of SYBR Green I. The results were analyzed using the Stratagene Mx3000 software, and the target mRNA levels were normalized to the level of *Actb* mRNA. The qPCR primer sequences were included in Table S3.

2.18. Statistical Analysis

The data was expressed as the means ± SD and was analyzed using GraphPad Prism (GraphPad Software, La Jolla, CA, USA). The mean and SD were presented in Tables S4–S21. For metabolomics analysis, the data was analyzed by MetaboAnalyst 3.0 [45]. For FCM analysis, the data was analyzed by FlowJo software (FlowJo, Ashland, OR, USA). Pearson's correlation analysis, One-way ANOVA with Tukey's multiple comparisons test (between multiple groups) and unpaired Student's *t*-test (between two groups) were used as appropriate. $P < 0.05$ was considered significant.

3. Results

3.1. Activation of Adipose Inflammasome Mediates Hcy-Induced Insulin Resistance

Human plasma was collected, and the level of Hcy was measured. Plasma Hcy levels were positively correlated with the homeostasis model assessment index of insulin resistance (HOMA-IR) (Fig. 1a). To investigate the precise mechanisms underlying the effects of Hcy on insulin resistance, WT mice were given Hcy in the drinking water, resulting in the elevation of plasma Hcy to pathophysiological concentrations (Fig. S1a). Body weights were not changed (Fig. S1b), but the GTT and ITT revealed a marked glucose intolerance and insulin resistance in the Hcy-treated mice (Fig. S1c, d). Plasma levels of IL12p70, MCP1 and IL6 were increased after 6-week of Hcy treatment (Fig. 1b). The expression of the macrophage marker mRNAs, *Emr1*, *Cd68* and *Cd11c*, were up-regulated in eWAT after Hcy treatment for 3 and 6 weeks (Fig. 1c), revealing increased ATM infiltration.

The plasma level of Hcy was positively correlated with plasma IL1β levels in humans (Fig. 1d). Consistent with this result, the plasma levels of IL1β were also progressively increased after Hcy-treatment for 3 and 6 weeks in mice (Fig. 1e). Therefore, activation of the adipose inflammasome in Hcy-treated mice was further examined. The *Casp1* mRNA expression was up-regulated after a 3-week-Hcy treatment, and the expression of *Nlrp3*, *Casp1* and *Il1b* mRNAs were all increased after 6-week-Hcy treatment in eWAT (Fig. 1f). However, the expression of *Nlrp3*, *Casp1* and *Il1b* mRNAs were not altered in inguinal white adipose tissue (iWAT) and brown adipose tissue (BAT) after Hcy treatment (Fig. S1e, f). The processing of CASP1 and the maturation of IL1β were further examined. Compared with vehicle-treated mice, the processing of CASP1 and the maturation of IL1β in eWAT were induced by Hcy treatment for 6 weeks (Fig. 1g).

To further examine involvement of inflammasome in Hcy-induced insulin resistance, *Casp1* mutant (*Casp1*$^{-/-}$) mice were employed [46]. The loss of effective *Casp1* was confirmed by genotyping PCR and qPCR analysis with primers targeting the mutated site (Fig. S2a, b). The CASP1 protein was almost undetectable in the *Casp1*$^{-/-}$ mice (Fig. S2c), which was a neoCASP1 fusion protein that did not contain the amino acid residues required for CASP1 enzymatic activity [47]. To clarify the contributions of adipocyte and ATM inflammasomes to Hcy-induced activation of the adipose inflammasome, BMT was performed. Bone marrow was isolated from WT and *Casp1*$^{-/-}$ mice, and was transplanted into WT and *Casp1*$^{-/-}$ mice to generate WT > WT, WT > *Casp1*$^{-/-}$, *Casp1*$^{-/-}$ > WT and *Casp1*$^{-/-}$ > *Casp1*$^{-/-}$ chimeric mice (Fig. S2d).

Genotyping PCR analysis of white blood cells and peripheral tissues confirmed that the BMT mice were highly chimeric (Fig. S2e). The chimeric mice were treated with Hcy in the drinking water for 6 weeks. Compared with WT > WT mice, the GTT and ITT revealed improved glucose intolerance and insulin resistance in the *Casp1*$^{-/-}$ > *Casp1*$^{-/-}$ mice. The improvement of insulin resistance in the *Casp1*$^{-/-}$ > *Casp1*$^{-/-}$ mice was substantially abolished in the *Casp1*$^{-/-}$ > WT mice but not in the WT > *Casp1*$^{-/-}$ mice (Fig. 1h, i), which indicated that Hcy-induced insulin resistance is primarily mediated by non-hematopoietic inflammasomes.

3.2. Hcy Activates the NLRP3 Inflammasome in Adipocytes

To further clarify the exact cell types that were responsible for the activation of inflammasomes in eWAT after Hcy treatment, the FLICA-CASP1 FCM analysis of adipocytes and SVF cells were employed (Fig. S3a). The percentages of active CASP1+ cells were increased in the SVF of 6-week-Hcy-treated mice, while the proportions of active CASP1+ adipocytes were increased after 3-week-Hcy treatment and remained elevated for 6 weeks (Fig. 2a), indicating that Hcy activates inflammasomes in both adipocytes and ATMs.

As bone marrow-derived macrophage inflammasomes seems not involved in Hcy-induced insulin resistance, the activation of adipocyte NLRP3 inflammasome by Hcy was further examined *in vitro*. Expression of the NLRP3 inflammasome components, *Nlrp3*, *Casp1* and *Il1b* mRNAs was up-regulated by Hcy in differentiated 3T3-L1 adipocytes (Fig. S3b). Hcy promoted the processing of CASP1 and the maturation of IL1β in LPS-primed 3T3-L1 adipocytes and rat primary adipocytes (Fig. 2b and Fig. S3c). Hcy elevated the activity of CASP1 in LPS-primed adipocytes (Fig. 2c). The secretion of IL1β was also increased by Hcy in LPS-primed 3T3-L1 and human adipocytes (Fig. 2d, e), while the secretion of TNFα remained unchanged (Fig. 2f). Glyburide was shown to inhibit activation of the NLRP3 inflammasome by blocking the PAMP- or DAMP-induced NLRP3 activation [48]. Hcy-induced IL1β secretion was inhibited after pretreatment with glyburide (Fig. 2g). These results reveal that Hcy activates the second signaling of the NLRP3 inflammasome in adipocytes.

3.3. Hcy Activates Adipose Phospholipids Metabolism and Lyso-PC Generation in vivo and in vitro

Compared with other second signal activators, including ATP, nigericin and uric acid [49,50], Hcy spends a longer time, approximately 16 h, on activating the NLRP3 inflammasome in adipocytes. This suggests that other mediators are involved in the Hcy-induced NLRP3 inflammasome activation in adipocytes. Lipids were identified as an important class of NLRP3 inflammasome second signal activators [17,18,51,52] and thus may mediate the Hcy-induced NLRP3 inflammasome activation in adipocytes. To determine the Hcy-induced changes in adipose lipid metabolism, a non-targeted lipidomics approach was performed *in vivo* and *in vitro*.

Partial least squares discriminant analysis (PLS-DA) of lipidomics data from eWAT of the 6-week-Hcy-treated mice had a lipid metabolic pattern distinct from the vehicle-treated mice (Fig. 3a). Variable importance in projection (VIP) scoring analysis further identified phospholipid and fatty acid (FA) metabolites that were among the top compounds, producing the separation (Fig. 3b). Heatmap of phospholipids

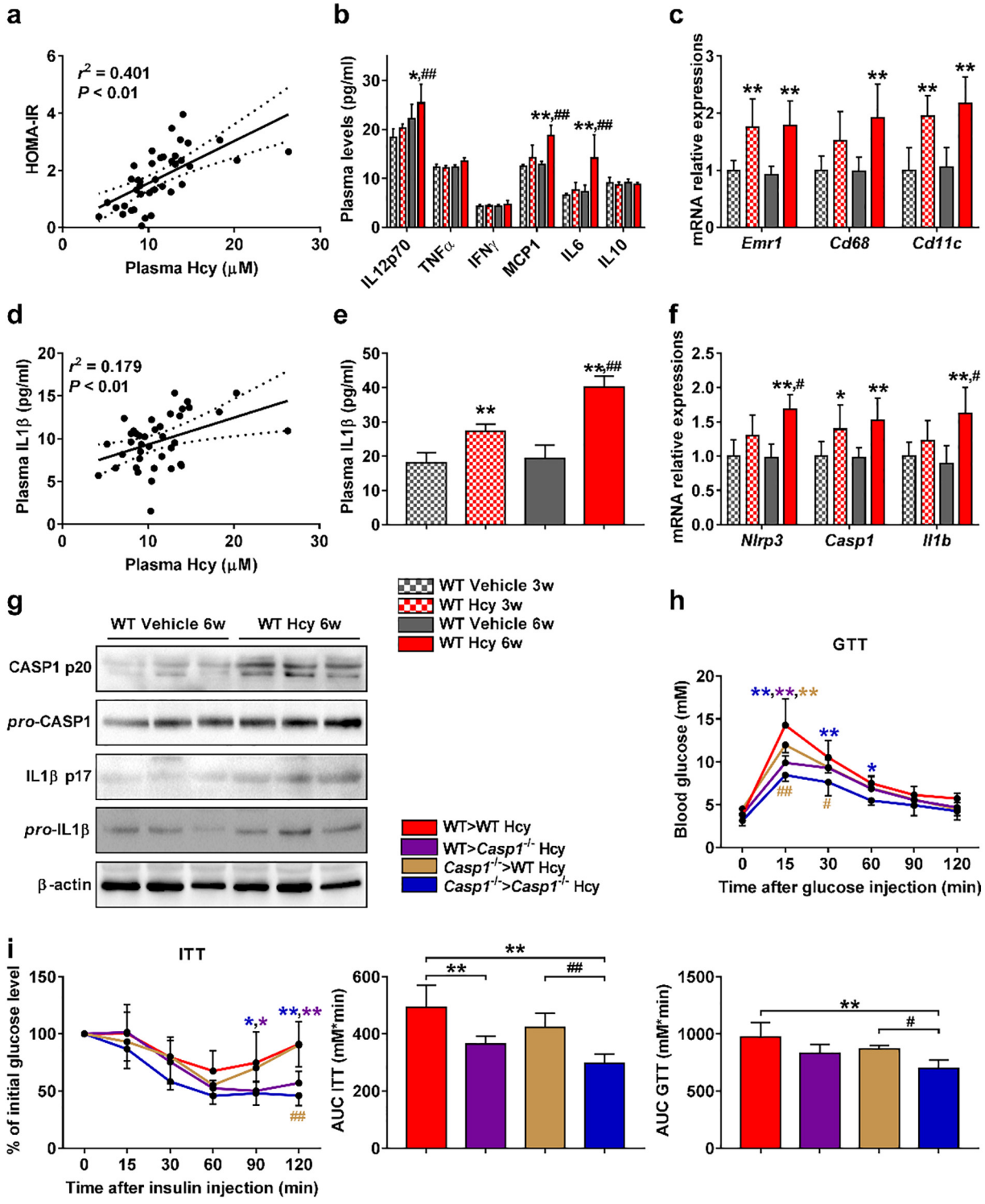

Fig. 1. Activation of adipose inflammasome mediates Hcy-induced insulin resistance. (a) Correlation analysis of plasma Hcy levels with HOMA-IR in human samples ($n = 39$ total individuals). (b) CBA analysis of plasma inflammatory cytokine levels ($n = 4$ per group). (c) qPCR analysis of the mRNA levels of *Emr1*, *Cd68* and *Cd11c* in eWAT ($n = 7$ per group). (d) Correlation analysis of plasma Hcy levels with plasma IL1β levels in human samples ($n = 39$ total individuals). (e) ELISA analysis of plasma IL1β levels ($n = 5$ per group). (f) qPCR analysis of the mRNA levels of *Nlrp3*, *Casp1* and *Il1b* in eWAT ($n = 7$ per group). (g) Western blot analysis of pro-CASP1, CASP1 p20, pro-IL1β and IL1β p17 protein levels in eWAT ($n = 6$ per group). (h) GTT of mice (upper panel) and AUC of GTT (lower panel) ($n = 5$–6 per group). (i) ITT of mice (left panel) and AUC of ITT (right panel) (n = 5–6 per group). (b, c, e–g) Seven-week-old WT mice were fed a normal chow diet and were given Hcy (1.8 g/l) or vehicle in the drinking water for 3 or 6 weeks. (h, i) Seven-week-old WT and *Casp1*$^{-/-}$ mice, transplanted with the bone marrow from WT or *Casp1*$^{-/-}$ mice, were fed a normal chow diet and were given Hcy (1.8 g/l) in the drinking water for 6 weeks. For qPCR analysis, the expressions were normalized to *Actb* mRNA. All data are presented as the means ± SD. (a, d) Pearson's correlation: $P < 0.01$ for HOMA-IR; $P < 0.01$ for IL1β. (b, c, e, f) One-way ANOVA with Tukey's correction: $^{*}P < 0.05$, $^{**}P < 0.01$ compared to the mice given vehicle in the drinking water; $\#P < 0.05$, $\#\#P < 0.01$ compared to the mice given Hcy in the drinking water for 3 weeks. (h, i) One-way ANOVA with Tukey's correction: $^{*}P < 0.05$, $^{**}P < 0.01$ compared to the WT > WT mice given Hcy in the drinking water for 6 weeks; $\#P < 0.05$, $\#\#P < 0.01$ compared to the *Casp1*$^{-/-}$ > *Casp1*$^{-/-}$ mice given Hcy in the drinking water for 6 weeks.

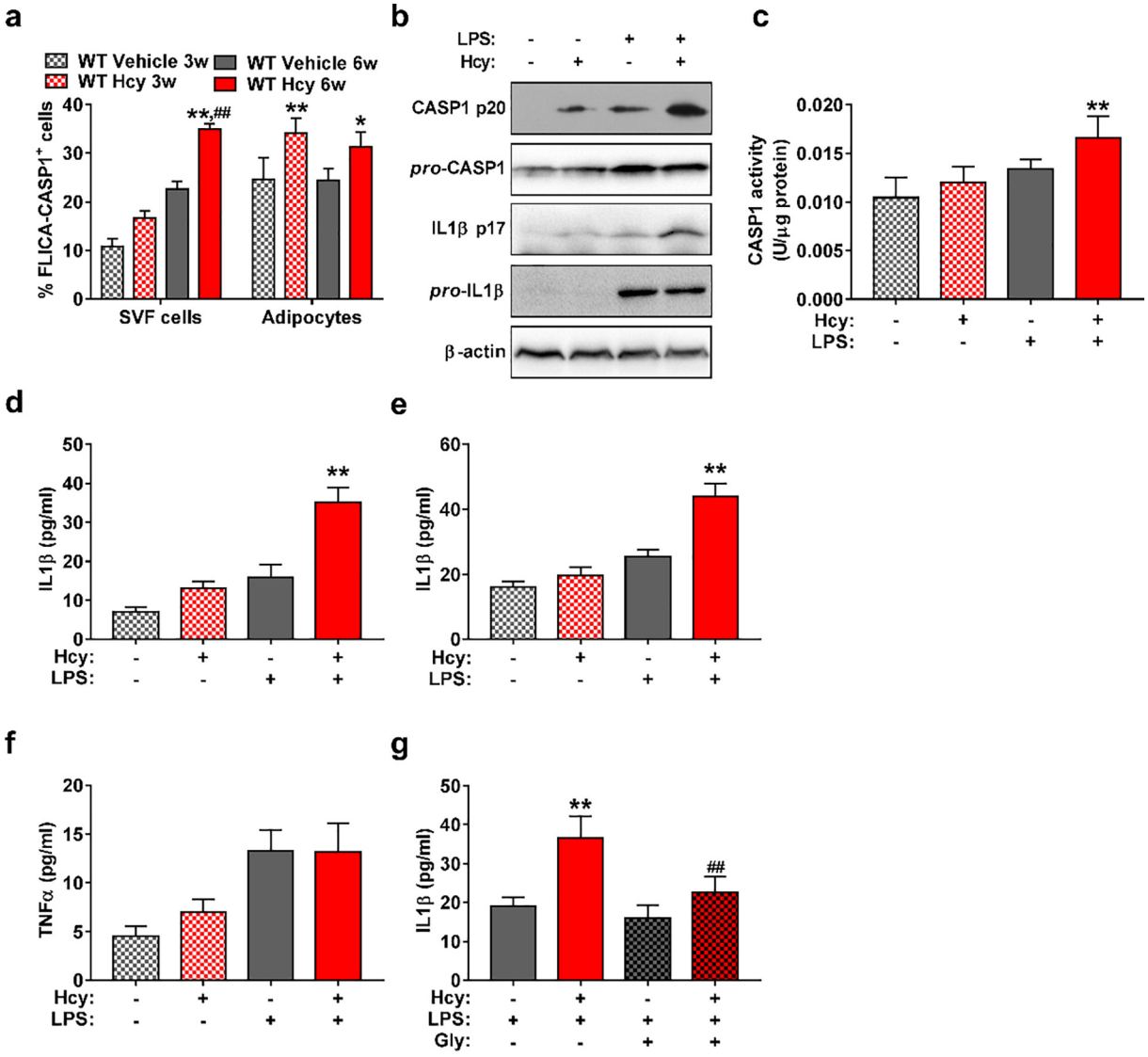

Fig. 2. Hcy activates the NLRP3 inflammasome in adipocytes. (a) FCM analysis of active Caspase1 in the SVF cells and adipocytes of eWAT by FLICA ($n = 3$; one sample was obtained from three independent experiments). (b) Western blot analysis of pro-CASP1, CASP1 p20, pro-IL1β and supernatant-IL1β p17 protein levels in differentiated 3T3-L1 adipocytes ($n = 4$ per group). (c) CASP1 activity of differentiated 3T3-L1 adipocytes ($n = 4$ per group). (d) ELISA analysis of supernatant IL1β levels of differentiated 3T3-L1 adipocytes ($n = 4$ per group). (e) ELISA analysis of supernatant IL1β levels of human differentiated adipocytes ($n = 4$ per group). (f) ELISA analysis of supernatant TNFα levels of differentiated 3T3-L1 adipocytes ($n = 4$ per group). (g) ELISA analysis of supernatant IL1β levels of differentiated 3T3-L1 adipocytes ($n = 4$ per group). (a) Seven-week-old WT mice were fed a normal chow diet and were given Hcy (1.8 g/l) or vehicle in the drinking water for 3 or 6 weeks. (b–g) Differentiated 3T3-L1 or human adipocytes were primed with LPS (1 μg/ml) for 3 h; after replacing the medium, the cells were treated with Hcy (500 μM) for another 16 h. (g) Differentiated 3T3-L1 adipocytes were primed with LPS (1 μg/ml) for 3 h; after replacing the medium, the cells were pretreated with glyburide (200 μM) for 0.5 h, followed by Hcy (500 μM) for another 16 h. All the data are presented as means ± SD. (a) One-way ANOVA with Tukey's correction: $^{*}P < 0.05$, $^{**}P < 0.01$ compared to the mice given vehicle in the drinking water; $\#\#P < 0.01$ compared to the mice given Hcy in the drinking water for 3 weeks. (c–g) One-way ANOVA with Tukey's correction: $^{*}P < 0.05$, $^{**}P < 0.01$ compared to the LPS-primed group; $\#\#P < 0.01$ compared to the LPS-primed Hcy treatment group.

and FAs showed increased lyso-PC and polyunsaturated fatty acid (PUFA) levels in the eWAT of Hcy-treated mice (Fig. 3c). The levels of lyso-PC (16:0), lyso-PC (18:0), lyso-PC (18:1) and lyso-PC (20:0), and the levels of FA (20:4) and FA (22:4) were increased by Hcy treatment (Fig. 3d, e). The generation of lyso-PC and PUFA depends on phospholipase A2 (PLA2), which hydrolyses the *sn*-2 position of phosphatidylcholine (PC) [53]. In agreement with the lipidomics data, PLA2 activity was elevated in the eWAT of Hcy-treated mice (Fig. 3f).

Lipidomics of differentiated human and 3T3-L1 adipocytes treated with Hcy *in vitro* were also performed. Heatmaps of phospholipids and FAs in the differentiated human and 3T3-L1 adipocytes displayed similar patterns as in the eWAT (Fig. 3g and Fig. S4a), suggesting that

Fig. 3. Hcy activates adipose phospholipid metabolism and lyso-PC generation *in vivo* and *in vitro*. (a) PLS-DA analysis of metabolites in eWAT ($n = 4$ per group). (b) VIP plot identified by PLS-DA showing the top 15 metabolites in eWAT ($n = 4$ per group). (c) Heatmap illustrating the phospholipid and FA metabolic profiles in eWAT ($n = 4$ per group). (d) HPLC-MS-MS analysis of different species of lyso-PC levels in eWAT ($n = 4$ per group). (e) HPLC-MS-MS analysis of different species of FA levels in eWAT ($n = 4$ per group). (f) PLA2 activity of eWAT ($n = 6$ per group). (g) Heatmap illustrating the phospholipid and FA metabolic profiles in differentiated human adipocytes ($n = 4$ per group). (h) HPLC-MS-MS analysis of different species of lyso-PC levels in differentiated human adipocytes ($n = 4$ per group). (i) HPLC-MS-MS analysis of different species of FA levels in differentiated human adipocytes ($n = 4$ per group). (j) PLA2 activity of differentiated human adipocytes ($n = 4$ per group). (a–f) Seven-week-old WT mice were fed a normal chow diet and were given Hcy (1.8 g/l) or vehicle in the drinking water for 6 weeks. (g–j) Differentiated human adipocytes treated with Hcy (500 μM) for 16 h. All the data are presented as means ± SD. (d–f) Two-tailed Student's *t*-test: $^{**}P < 0.01$ compared to the mice given vehicle in the drinking water. (h–j) Two-tailed Student's *t*-test: $^{*}P < 0.05$, $^{**}P < 0.01$ compared to the control group.

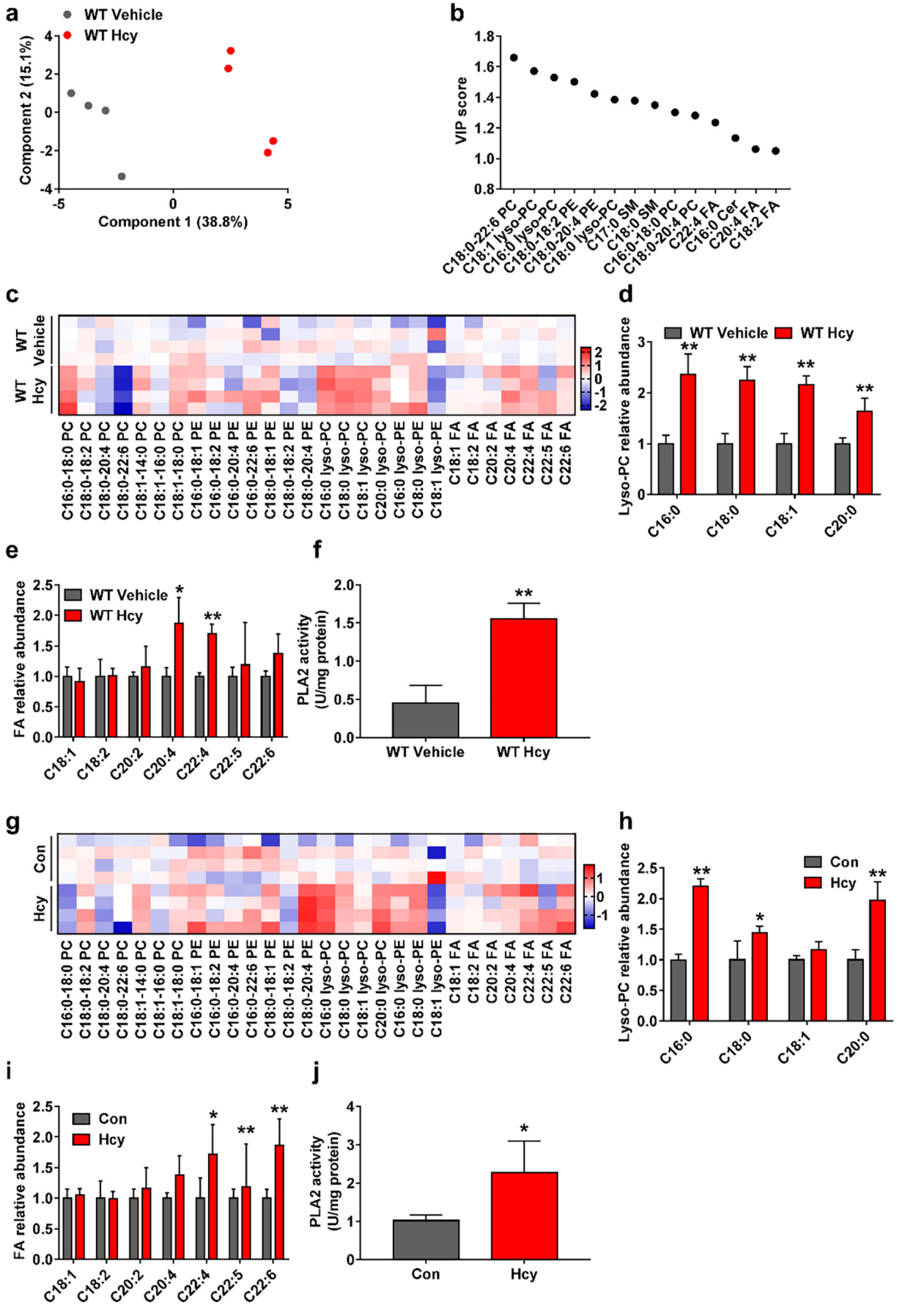
a
WT Vehicle
WT Hcy
Component 2 (15.1%)
Component 1 (38.8%)
b
VIP score
C18:0-22:6 PC
C18:1 lyso-PC
C16:0 lyso-PC
C18:0-18:2 PE
C18:0-20:4 PE
C18:0 lyso-PC
C17:0 SM
C18:0 SM
C16:0-18:0 PC
C18:0-20:4 PC
C22:4 FA
C16:0 Cer
C20:4 FA
C18:2 FA
c
WT Vehicle
WT Hcy
C16:0-18:0 PC
C18:0-18:2 PC
C18:0-20:4 PC
C18:0-22:6 PC
C18:1-14:0 PC
C18:1-16:0 PC
C18:1-18:0 PC
C16:0-18:1 PE
C16:0-18:2 PE
C16:0-20:4 PE
C16:0-22:6 PE
C18:0-18:1 PE
C18:0-18:2 PE
C18:0-20:4 PE
C16:0 lyso-PC
C18:0 lyso-PC
C18:1 lyso-PC
C20:0 lyso-PC
C16:0 lyso-PE
C18:0 lyso-PE
C18:1 lyso-PE
C18:1 FA
C18:2 FA
C20:2 FA
C20:4 FA
C22:4 FA
C22:5 FA
C22:6 FA
d
WT Vehicle
WT Hcy
Lyso-PC relative abundance
C16:0
C18:0
C18:1
C20:0
e
WT Vehicle
WT Hcy
FA relative abundance
C18:1
C18:2
C20:2
C20:4
C22:4
C22:5
C22:6
f
PLA2 activity (U/mg protein)
WT Vehicle
WT Hcy
g
Con
Hcy
h
Con
Hcy
Lyso-PC relative abundance
C16:0
C18:0
C18:1
C20:0
i
Con
Hcy
FA relative abundance
C18:1
C18:2
C20:2
C20:4
C22:4
C22:5
C22:6
j
PLA2 activity (U/mg protein)
Con
Hcy

the metabolic changes in the eWAT of the Hcy-treated mice originated primarily from adipocytes. Consistent with the eWAT, the levels of lyso-PC (16:0), lyso-PC (18:0) and lyso-PC (20:0) in the human adipocytes, and lyso-PC (16:0), lyso-PC (18:0), lyso-PC (18:1) and lyso-PC (20:0) in the 3T3-L1 adipocytes were increased after Hcy treatment (Fig. 3h and Fig. S4b). The levels of FA (22:4), FA (22:5) and FA (22:6) in the human, and FA (22:4) and FA (22:6) in the 3T3-L1 adipocytes were also elevated after Hcy treatment (Fig. 3i and Fig. S4c). Hcy increased the PLA2 activity in both human, and 3T3-L1 adipocytes in a time-dependent manner (Fig. 3j and Fig. S4d). These results indicated that Hcy promotes adipose lyso-PC and PUFA generation through increasing PLA2 activity *in vivo* and *in vitro*.

3.4. Hcy Promotes Adipocyte Lyso-PC Generation and Inflammasome Activation via Up-Regulation of PLA2G16

To clarify the mechanism of Hcy-induced lyso-PC generation and increased PLA2 activity, the expression of genes involved in the Land's cycle were examined. The mRNA and protein levels of PLA2G16 were increased in the eWAT of Hcy-treated mice (Fig. 4a, b). PLA2G16 is a PLA2

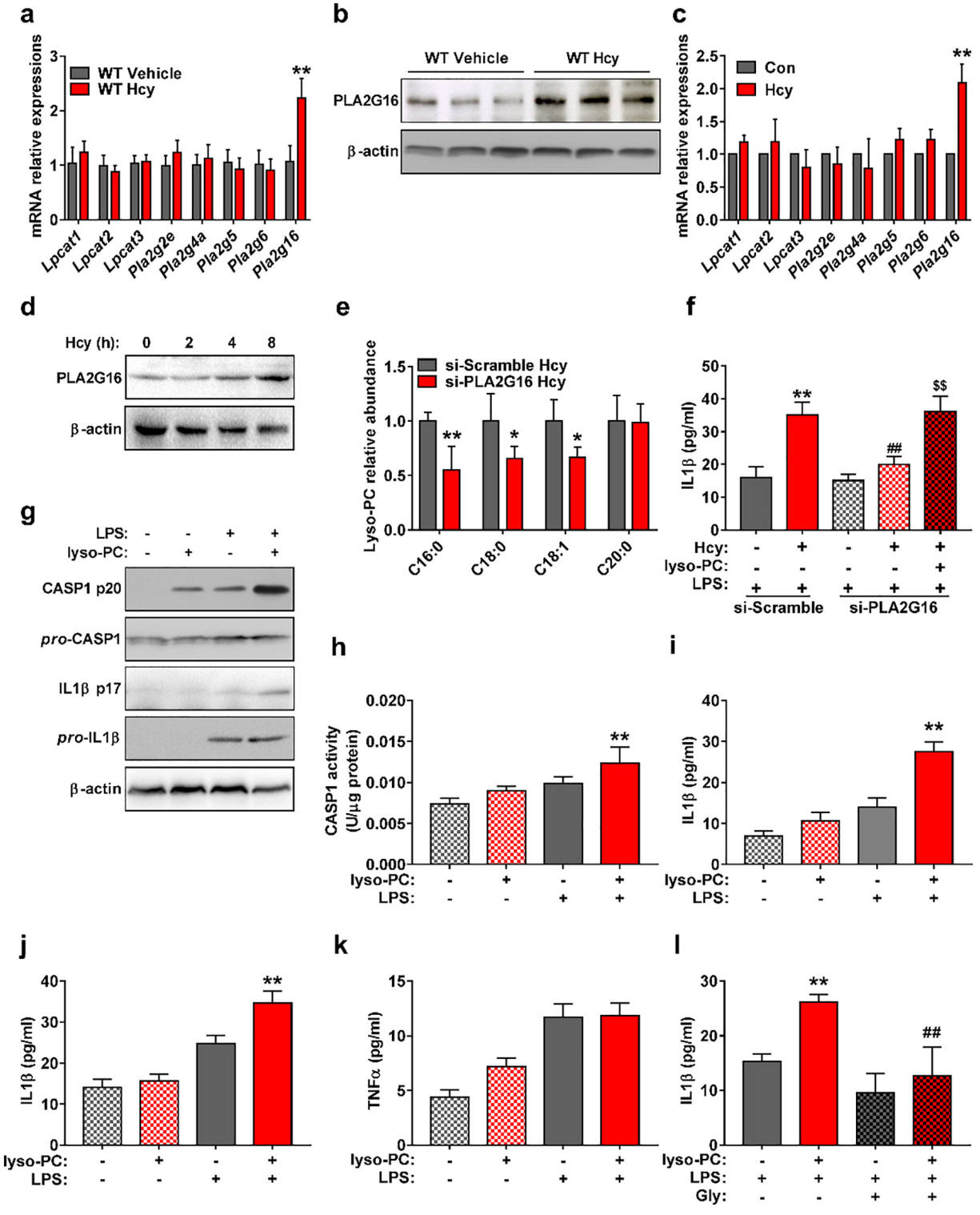

and is specifically expressed in adipocytes with a preference toward hydrolyze PC [54]. The mRNA and protein expression of PLA2G16 was also up-regulated in 3T3-L1 and human adipocytes *in vitro* after Hcy treatment (Fig. 4c, d and Fig. S5a). The expression of *Pla2g16* was knocked down by transfecting si-PLA2G16 into differentiated 3T3-L1 adipocytes (Fig. S5b, c). The PLA2 activity of the adipocytes was decreased after PLA2G16 knockdown (Fig. S5d). Lipidomics results revealed that the Hcy-induced lyso-PC (16:0), lyso-PC (18:0) and lyso-PC (18:1) were inhibited by PLA2G16 knockdown (Fig. 4e). The secretion of IL1β, triggered by Hcy, was also decreased by si-PLA2G16 transfection, which was reversed by the administration of lyso-PC (16:0) in LPS-primed 3T3-L1 adipocytes (Fig. 4f).

Whether lyso-PC acts as a second signal activator of the NLRP3 inflammasome was further examined in adipocytes. Lyso-PC (16:0) promoted the processing of CASP1 and the maturation of IL1β in LPS-primed 3T3-L1 adipocytes and rat primary adipocytes (Fig. 4g and Fig. S5e). Lyso-PC (16:0) increased the activity of CASP1 in LPS-primed adipocytes (Fig. 4h). The secretion of IL1β was also elevated by lyso-PC (16:0) in LPS-primed 3T3-L1 and human adipocytes (Fig. 4i, j), but the secretion of TNFα was not changed (Fig. 4k). IL1β secretion, induced by lyso-PC (16:0), was inhibited by glyburide treatment (Fig. 4l). These results indicate that Hcy up-regulates PLA2G16 expression in adipocytes, which mediates the Hcy-induced lyso-PC generation and inflammasome activation.

3.5. Adipocyte HIF1 Mediates Hcy-Induced Adipose PLA2G16 Expression and Lyso-PC Generation

To determine the mechanism underlying the Hcy-induced up-regulation of PLA2G16, the murine *Pla2g16* gene sequence was retrieved from the GenBank genome database, and the existence of potential transcription factor binding sites were analyzed. A HRE was identified in the first intron of *Pla2g16* near the transcription initiation site (Fig. S6a). The expression of *Pla2g16* mRNA was increased in the eWAT of *Hif1a*^{LSL} mice (Fig. 5a and Fig. S6b, c).

Hcy was previously shown to increase the HIF1α protein levels of podocytes [55]. An increased HIF1α protein was also observed in the eWAT of Hcy-treated mice (Fig. 5b). Therefore, the involvement of HIF1 in Hcy-induced PLA2G16 expression was further examined. Treatment with ACF, a HIF1α and β dimerization inhibitor [56], was found to abolish the Hcy-induced *Pla2g16* mRNA expression (Fig. 5c). The expression of *Pla2g16* mRNA was also reduced in the eWAT of Hcy-treated *Hif1a*$^{\Delta Ad}$ mice (Fig. 5d, e and Fig. S6d, e). ChIP assays identified the binding of HIF1α to the HRE of *Pla2g16* in the Hcy-treated adipocytes (Fig. 5f). Luciferase reporter assays also showed that *Pla2g16* promoter activity was increased after HIF1α transfection (Fig. 5g), indicating that *Pla2g16* is a direct HIF1 target gene.

In line with the down-regulation of PLA2G16 expression, the PLA2 activity of eWAT was also decreased in the Hcy-treated *Hif1a*$^{\Delta Ad}$ mice (Fig. 5h). Lipidomics analysis was performed in the eWAT of Hcy-treated *Hif1a*$^{\Delta Ad}$ mice. The levels of lyso-PC (16:0), lyso-PC (18:1) and lyso-PC (20:0) were decreased (Fig. 5i), while the levels of FA were not changed in the *Hif1a*$^{\Delta Ad}$ mice (Fig. 5j).

3.6. Hcy-Induced Insulin Resistance and Adipose Inflammasome Activation Are Improved in the *Hif1a*$^{\Delta Ad}$ Mice

The Hcy-induced insulin resistance and adipose inflammasome activation were also evaluated in Hcy-treated *Hif1a*$^{fl/fl}$ and *Hif1a*$^{\Delta Ad}$ mice. The GTT and ITT showed improvement of Hcy-induced glucose intolerance and insulin resistance in *Hif1a*$^{\Delta Ad}$ mice (Fig. 6a, b). The plasma levels of the pro-inflammatory cytokines TNFα, IFNγ and MCP1 were decreased in the Hcy-treated *Hif1a*$^{\Delta Ad}$ mice (Fig. 6c). Expression of the pro-inflammatory macrophage marker *Cd11c* mRNA was also decreased in the eWAT of *Hif1a*$^{\Delta Ad}$ mice, but the total macrophage marker mRNAs *Emr1* and *Cd68* expression were not changed (Fig. 6d). The expression of pro-inflammatory cytokine mRNAs, *Tnf*, *Ccl5* and *Pai1*, was down-regulated in the eWAT of Hcy-treated *Hif1a*$^{\Delta Ad}$ mice (Fig. 6e).

The plasma levels of IL1β were decreased in *Hif1a*$^{\Delta Ad}$ mice after Hcy treatment (Fig. 6f). The Hcy-induced NLRP3 inflammasome component, *Nlrp3*, *Casp1* and *Il1b*, mRNAs expression was also down-regulated in the eWAT of *Hif1a*$^{\Delta Ad}$ mice (Fig. 6g). The processing of CASP1 and the maturation of IL1β in the eWAT were inhibited in the *Hif1a*$^{\Delta Ad}$ mice treated with Hcy (Fig. 6h). Activation of the inflammasomes was further examined by FLICA-CASP1 FCM. Interestingly, the adipocyte-specific knockout of *Hif1a* decreased the active CASP1 levels in both adipocytes and ATMs treated with Hcy (Fig. 6i), indicating that the HIF1-PLA2G16 axis in adipocytes is responsible for the Hcy-induced inflammasome activation in both adipocytes and ATMs.

3.7. Adipocyte-Derived Lyso-PC Activates the NLRP3 Inflammasome in Macrophages

The participation of the adipocyte HIF1-PLA2G16 axis in the Hcy-induced activation of both adipocyte and ATM inflammasomes suggested that the adipocyte-derived lyso-PC could act as a lipokine, activating the second signaling of ATM NLRP3 inflammasome in a paracrine manner. Conditioned medium (CM), collected from Hcy-treated adipocytes, triggered IL1β secretion in the LPS-primed macrophages (Fig. 7a). To rule out the effects of peptides or hydrophilic molecules in the CM on macrophage inflammasome activation, the lipid content was extracted from the CM as an organic extract (OE). The OE from Hcy-treated adipocytes also promoted IL1β secretion in the LPS-primed macrophages (Fig. 7a).

Fig. 4. Hcy promotes adipocyte lyso-PC generation and inflammasome activation *via* up-regulation of PLA2G16. (a) qPCR analysis of the mRNA levels of *Lpcat1*, *Lpcat2*, *Lpcat3*, *Pla2g2e*, *Pla2g4a*, *Pla2g5*, *Pla2g6* and *Pla2g16* in eWAT ($n = 7$ per group). (b) Western blot analysis of PLA2G16 protein levels in eWAT ($n = 6$ per group). (c) qPCR analysis of the mRNA levels of *Lpcat1*, *Lpcat2*, *Lpcat3*, *Pla2g2e*, *Pla2g4a*, *Pla2g5*, *Pla2g6* and *Pla2g16* in differentiated 3T3-L1 adipocytes ($n = 4$ per group). (d) Western blot analysis of PLA2G16 protein levels in differentiated 3T3-L1 adipocytes ($n = 4$ per group). (e) HPLC-MS-MS analysis of different species of lyso-PC levels in differentiated 3T3-L1 adipocytes ($n = 4$ per group). (f) ELISA analysis of supernatant IL1β levels of differentiated 3T3-L1 adipocytes ($n = 4$ per group). (g) Western blot analysis of pro-CASP1, CASP1 p20, pro-IL1β and supernatant-IL1β p17 protein levels in differentiated 3T3-L1 adipocytes ($n = 4$ per group). (h) CASP1 activity of differentiated 3T3-L1 adipocytes ($n = 4$ per group). (i) ELISA analysis of supernatant IL1β levels of differentiated 3T3-L1 adipocytes ($n = 4$ per group). (j) ELISA analysis of supernatant IL1β levels of differentiated human adipocytes ($n = 4$ per group). (k) ELISA analysis of supernatant TNFα levels of differentiated 3T3-L1 adipocytes ($n = 4$ per group). (l) ELISA analysis of supernatant IL1β levels of differentiated 3T3-L1 adipocytes ($n = 4$ per group). (a, b) Seven-week-old WT mice were fed a normal chow diet and were given Hcy (1.8 g/l) or vehicle in the drinking water for 6 weeks. (c) Differentiated 3T3-L1 adipocytes were given Hcy (500 μM) for 8 h. (d) Differentiated 3T3-L1 adipocytes were given Hcy (500 μM) for indicated hours. (e) Differentiated 3T3-L1 adipocytes were transfected with si-Scramble or si-PLA2G16 for 36 h, and the cells were treated with Hcy (500 μM) for 16 h. (f) Differentiated 3T3-L1 adipocytes were transfected with si-Scramble or si-PLA2G16 for 36 h. The cells were then primed with LPS (1 μg/ml) for 3 h; after replacing the medium, the cells were treated with Hcy (500 μM) for another 16 h, followed by lyso-PC (16:0) (20 μM) for additional 3 h. (g–k) Differentiated 3T3-L1 or human adipocytes were primed with LPS (1 μg/ml) for 3 h; after replacing the medium, the cells were treated with lyso-PC (16:0) (20 μM) for another 3 h. (l) Differentiated 3T3-L1 adipocytes were primed with LPS (1 μg/ml) for 3 h; after replacing the medium, the cells were pretreated with glyburide (200 μM) for 0.5 h, followed by lyso-PC (16:0) (20 μM) for another 3 h. For qPCR analysis, the expression were normalized to *Actb* mRNA. All the data are presented as means ± SD. (a) Two-tailed Student's *t*-test: $^{**}P < 0.01$ compared to the mice given vehicle in the drinking water. (c) Two-tailed Student's *t*-test: $^{**}P < 0.01$ compared to the control group. (e) Two-tailed Student's *t*-test: $^{*}P < 0.05$, $^{**}P < 0.01$ compared to the si-Scramble transfected group. (f) One-way ANOVA with Tukey's correction: $^{**}P < 0.01$ compared to the si-Scramble transfected LPS-primed control group; $\#\#P < 0.01$ compared to the si-Scramble transfected LPS-primed Hcy treatment group; $\$\$P < 0.01$ compared to the si-PLA2G16 transfected LPS-primed Hcy treatment group. (h–l) One-way ANOVA with Tukey's correction: $^{**}P < 0.01$ compared to the LPS-primed group; $\#\#P < 0.01$ compared to the LPS-primed lyso-PC treatment group.

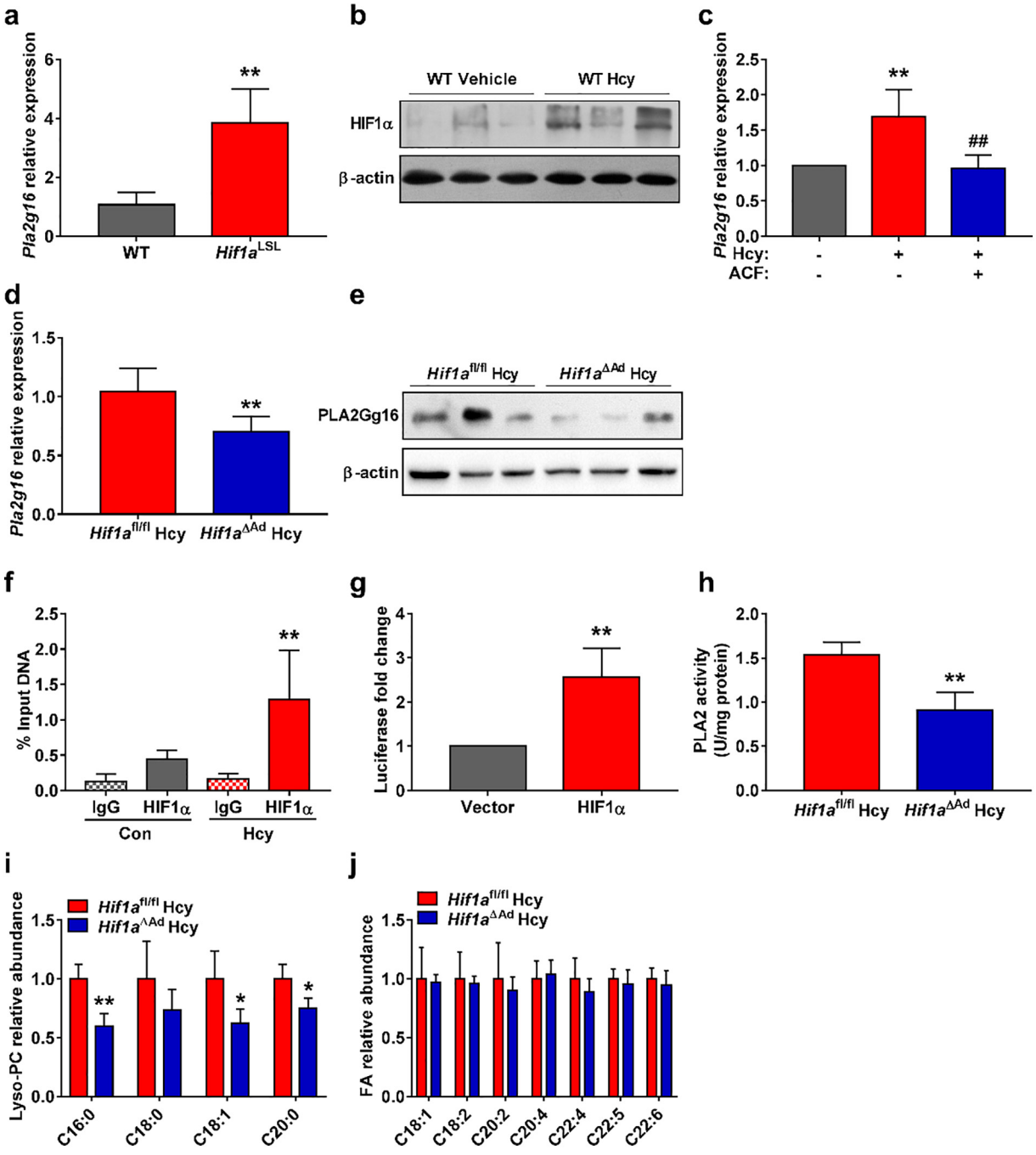

Fig. 5. Adipocyte HIF1 mediates Hcy-induced adipose PLA2G16 expression and lyso-PC generation. (a) qPCR analysis of the mRNA levels of *Pla2g16* in eWAT ($n = 7$ per group). (b) Western blot analysis of HIF1α protein level in eWAT ($n = 6$ per group). (c) qPCR analysis of the mRNA levels of *Pla2g16* in differentiated 3T3-L1 adipocytes ($n = 4$ per group). (d) qPCR analysis of the mRNA levels of *Pla2g16* in eWAT ($n = 7$ per group). (e) Western blot analysis of PLA2g16 protein level in eWAT ($n = 6$ per group). (f) ChIP-qPCR analysis of the binding of HIF1α to the HRE region of *Pla2g16* ($n = 9$ per group). (g) Luciferase assay of *Pla2g16* transcription activity ($n = 6$ per group). (h) PLA2 activity of eWAT ($n = 7$ per group). (i) HPLC-MS-MS analysis of the different species of lyso-PC levels in eWAT ($n = 4$ per group). (j) HPLC-MS-MS analysis of different species of FA levels in eWAT ($n = 4$ per group). (a) Seven-week-old WT and *Hif1a*^{LSL} mice were fed a normal chow diet. (b) Seven-week-old WT mice were fed a normal chow diet and were given Hcy (1.8 g/l) or vehicle in the drinking water for 6 weeks. (c) Differentiated 3T3-L1 adipocytes were pretreated with ACF (2 μM) for 0.5 h, followed with Hcy (500 μM) for another 8 h. (d, e, h–j) Seven-week-old *Hif1a*$^{fl/fl}$ and *Hif1a*$^{\Delta Ad}$ mice were fed a normal chow diet and were given Hcy (1.8 g/l) in the drinking water for 6 weeks. (f) Differentiated 3T3-L1 adipocytes were treated with Hcy (500 μM) for 4 h. (g) 293T cells were co-transfected with the *Pla2g16* promoter luciferase reporter gene and vector or HIF1α plasmid for 24 h. For qPCR analysis, the expressions were normalized to *Actb* mRNA. For ChIP analysis, the expressions were normalized to the input. All data are presented as the means ± SD. (a) Two-tailed Student's *t*-test: $^{**}P < 0.01$ compared to the WT mice. (b) One-way ANOVA with Tukey's correction: $^{**}P < 0.01$ compared to the control group; $\#\#P < 0.01$ compared to the Hcy treatment group. (d, h–j) Two-tailed Student's *t*-test: $^{*}P < 0.05$, $^{**}P < 0.01$ compared to the *Hif1a*$^{fl/fl}$ mice given Hcy in the drinking water. (f) Two-tailed Student's *t*-test: $^{**}P < 0.01$ compared to the control group with HIF1α antibody pull-down. (g) Two-tailed Student's *t*-test: $^{**}P < 0.01$ compared to the vector transfected group.

To determine whether lyso-PC acts as a second signal activator of macrophage NLRP3 inflammasomes, LPS-primed macrophages were treated with lyso-PC (16:0). Lyso-PC (16:0) increased the processing of CASP1 and the maturation of IL1β in LPS-primed macrophages (Fig. 7b). The activity of CASP1 (Fig. 7c) and the secretion of IL1β (Fig. 7d) were also increased by lyso-PC (16:0) in LPS-primed macrophages, whereas the secretion of TNFα was unchanged (Fig. 7e). The lyso-PC (16:0)-triggered IL1β secretion in the LPS-primed macrophages

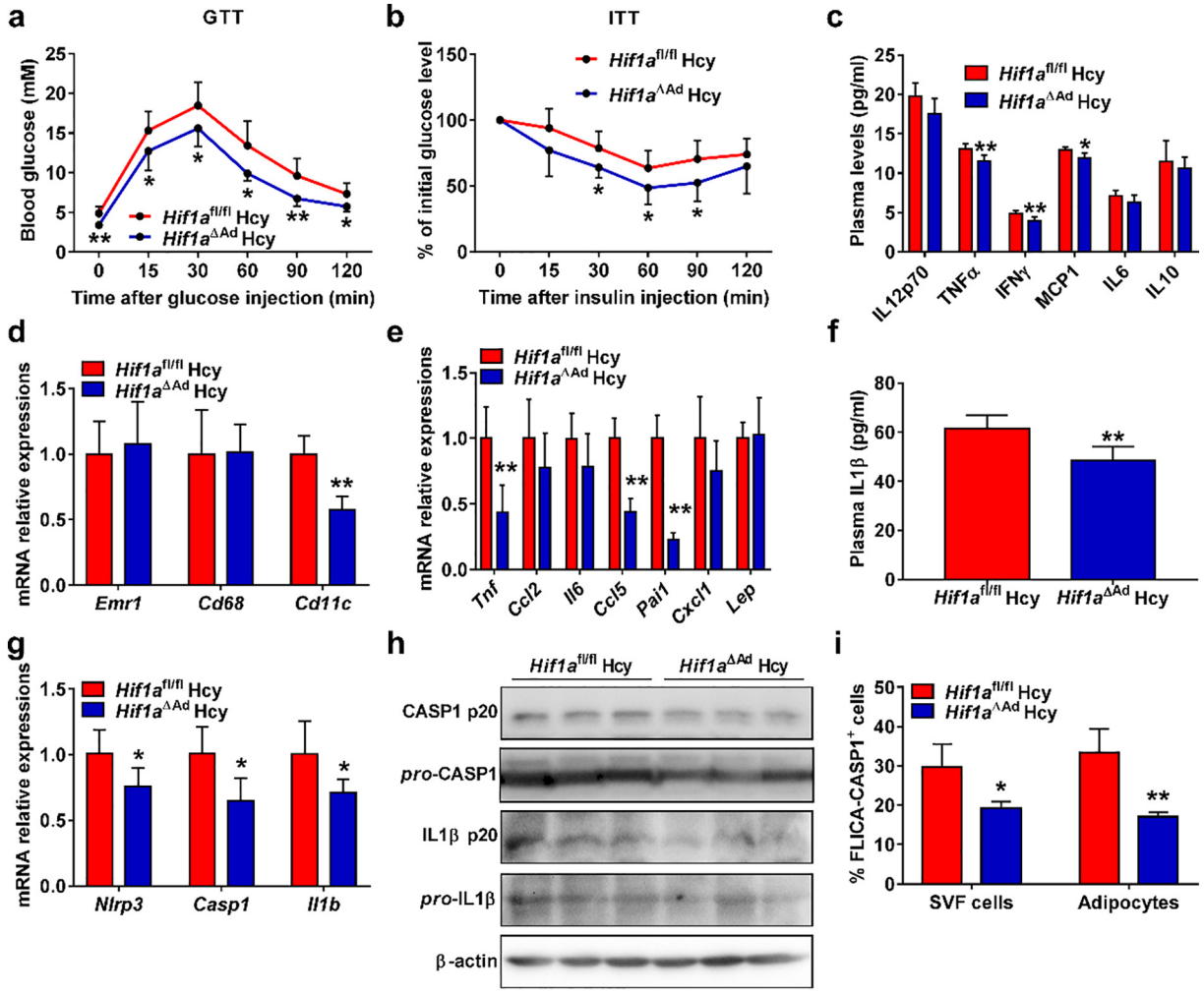

Fig. 6. Hcy-induced insulin resistance and adipose inflammasome activation are improved in the *Hif1a*$^{\Delta Ad}$ mice. (a) GTT of mice ($n = 7$–10 per group). (b) ITT of mice ($n = 7$–9 per group). (c) CBA analysis of plasma inflammatory cytokine levels ($n = 5$ per group). (d) qPCR analysis of the mRNA levels of *Emr1*, *Cd68* and *Cd11c* in eWAT ($n = 4$–5 per group). (e) qPCR analysis of the mRNA levels of *Tnf*, *Ccl2*, *Il6*, *Ccl5*, *Pai1*, *Cxcl1* and *Lep* in eWAT ($n = 4$–5 per group). (f) ELISA analysis of plasma IL1β levels ($n = 6$ per group). (g) qPCR analysis of the mRNA levels of *Nlrp3*, *Casp1* and *Il1b* in eWAT ($n = 5$ per group). (h) Western blot analysis of pro-CASP1, CASP1 p20, pro-IL1β and IL1β p17 protein levels in eWAT ($n = 6$ per group). (i) FCM analysis of active CASP1 in the SVF cells and adipocytes of eWAT by FLICA ($n = 4$, one sample was obtained from three independent experiments). (a–i) Seven-week-old *Hif1a*$^{fl/fl}$ and *Hif1a*$^{\Delta Ad}$ mice were fed a normal chow diet and were given Hcy (1.8 g/l) in the drinking water for 6 weeks. For qPCR analysis, the expressions were normalized to *Actb* mRNA. All the data are presented as means ± SD. (a-g, i) Two-tailed Student's *t*-test: $^{*}P < 0.05$, $^{**}P < 0.01$ compared to the *Hif1a*$^{fl/fl}$ mice given Hcy in the drinking water.

was abolished by glyburide treatment (Fig. 7f). These results indicate that lyso-PC derived from adipocytes, activates the second signaling of the NLRP3 inflammasome in macrophages.

4. Discussion

In this study, human HOMA-IR was positively associated with plasma Hcy levels, consistent with previous studies [24–26]. A positive association between plasma IL1β and Hcy levels was further observed in humans. IL1β is one of the master regulators of both innate and adaptive immunity [57], linking inflammasome activation with insulin resistance [58]. IL1β down-regulates insulin receptor substrate 1 expression, inhibiting insulin-induced AKT phosphorylation and glucose uptake in adipocytes [59]. *Il1b* knockout mice are protected from high-fat diet-induced insulin resistance, while IL1β infusion exacerbates insulin resistance [15,18]. The eWAT expression of *Il1b* mRNA and the plasma levels of IL1β were increased in the Hcy-treated mice, indicating that IL1β is one of the mediators involved in Hcy-induced insulin resistance. The maturation of IL1β relies on the inflammasomes [10]. The expression of NLRP3 inflammasome components and the cleavage of CASP1 and IL1β were increased in the eWAT of Hcy-treated mice. Furthermore, the Hcy-induced insulin resistance was improved in the *Casp1*$^{-/-}$ > *Casp1*$^{-/-}$ mice, indicating the participation of inflammasome activation in Hcy-induced insulin resistance.

Adipose tissue is a mixture of adipocytes, adipose immune cells, adipose progenitor cells and vasculature. However, the cell types responsible for adipose inflammasome activation and insulin resistance remain to be clarify. The macrophage NLRP3 inflammasome is found to mediate high-fat diet-induced insulin resistance [18]. In adipose tissue, the ATM NLRP3 inflammasome is activated after high-fat diet treatment and promotes insulin resistance and adipose inflammation [17]. However, expression and activation of the inflammasome are also observed in human and murine primary adipocytes [60] and are closely associated with obesity-induced adipose inflammation in humans [20]. In this study, FLICA-CASP1 FCM was performed to measure activation of CASP1 in adipocytes and ATMs at the same time *in vivo*, and the BMT was also used to compare the contributions of hematopoietic and non-hematopoietic inflammasomes to insulin resistance. The inflammasomes were activated in both adipocytes and ATMs, but the activation of adipocyte inflammasomes occurred earlier. Bone marrow-derived macrophage inflammasomes seem not involved in Hcy-induced insulin resistance. Consistent with the present results,

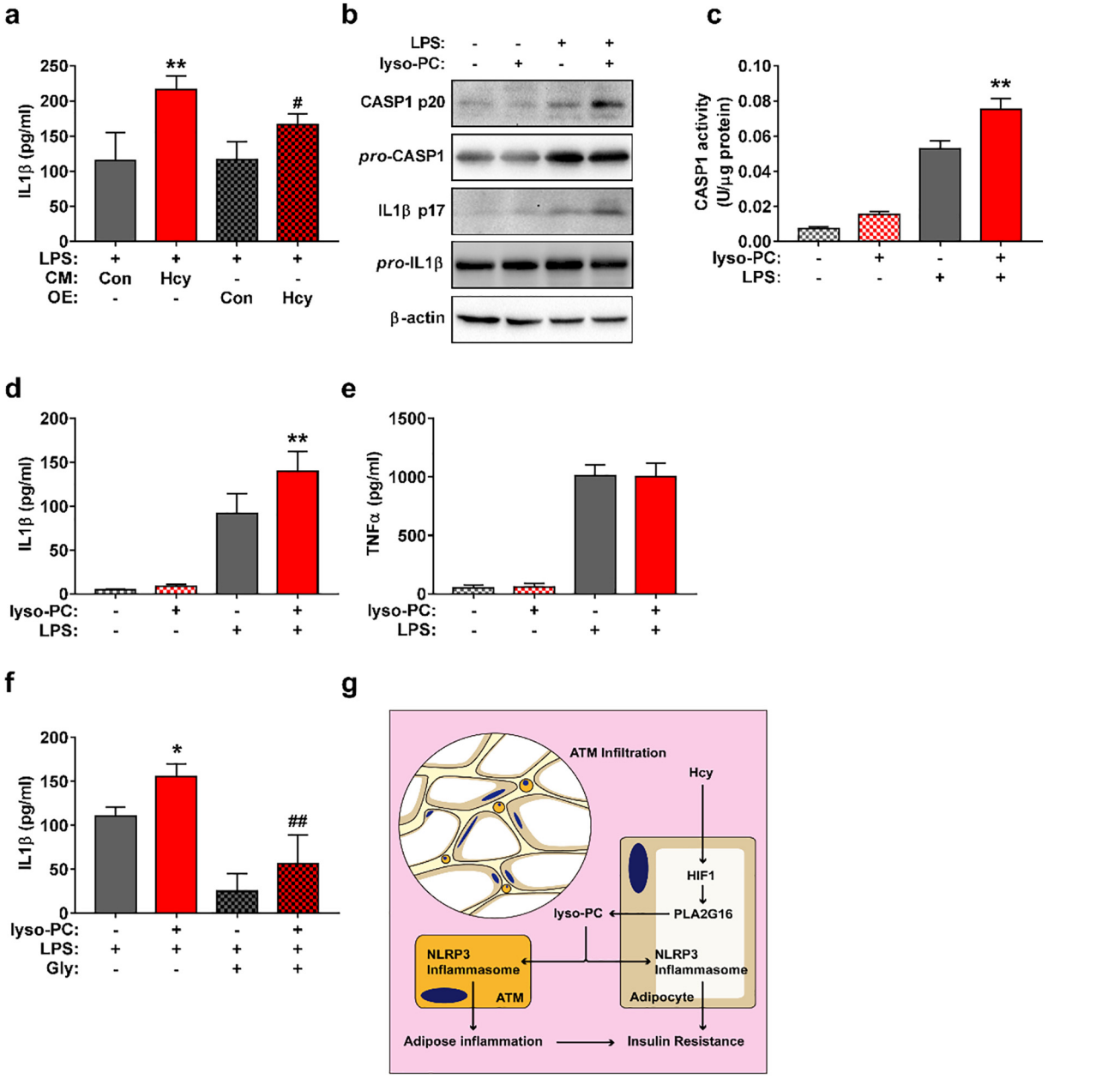

Fig. 7. Adipocyte-derived lyso-PC activates the NLRP3 inflammasome in macrophages. (a) ELISA analysis of supernatant IL1β levels of peritoneal macrophages ($n = 4$ per group). (b) Western blot analysis of pro-CASP1, CASP1 p20, pro-IL1β and supernatant-IL1β p17 protein levels in peritoneal macrophages ($n = 4$ per group). (c) CASP1 activity of peritoneal macrophages ($n = 4$ per group). (d) ELISA analysis of supernatant IL1β levels of peritoneal macrophages ($n = 6$ per group). (e) ELISA analysis of supernatant TNFα levels of peritoneal macrophages ($n = 6$ per group). (f) ELISA analysis of supernatant IL1β levels of peritoneal macrophages ($n = 6$ per group). (g) Scheme summarizing the activation of adipose NLRP3 inflammasome by adipocyte-derived lyso-PC in the Hcy-induced insulin resistance. (a) Peritoneal macrophages were primed with LPS (0.5 μg/ml) for 3 h; after replacing the medium, the cells were treated with CM or OE from the conditioned medium of 3T3-L1 adipocytes treated with Hcy (500 μM). (b–e) Peritoneal macrophages were primed with LPS (0.5 μg/ml) for 3 h; after replacing the medium, the cells were treated with lyso-PC (16:0) (20 μM) for another 1 h. (f) Peritoneal macrophages were primed with LPS (0.5 μg/ml) for 3 h; after replacing the medium, the cells were pretreated with glyburide (200 μM) for 0.5 h, followed by lyso-PC (16:0) (20 μM) for another 1 h. For qPCR analysis, the expressions were normalized to *Actb* mRNA. All the data are presented as means ± SD. (a) One-way ANOVA with Tukey's correction: $^{**}P < 0.01$ compared to the LPS-primed control CM treatment group; $\#P < 0.05$ compared to the LPS-primed control OE treatment group. (b–f) One-way ANOVA with Tukey's correction: $^{*}P < 0.05$, $^{**}P < 0.01$ compared to the LPS-primed group; $\#\#P < 0.01$ compared to the LPS-primed lyso-PC treatment group.

Casp1$^{-/-}$ mice has been shown to promote plasma triglyceride clearance in a non-hematopoietic cell-dependent manner and does not rely on IL1β [61]. IL1β and IL18 are not the only substrates of CASP1. Sirtuin1, a NAD^+-dependent deacetylase regulating lipid metabolism, was reported to be cleaved by CASP1 in adipose tissue after high-fat diet treatment [62]. Peroxisome proliferator activated receptor γ (PPARγ), a nuclear receptor involved in insulin sensitization, is also cleaved by CASP1, influencing FA storage and mitochondrial function [63]. Therefore, the adipocyte inflammasome may promote insulin resistance in both IL1β-dependent and independent manners.

Although activation of the NLRP3 inflammasome in adipocytes was observed in previous studies, the endogenous second signal activators has not been reported. In this study, Hcy was found to activate the second signaling of NLRP3 inflammasomes and up-regulate the expression of NLRP3 inflammasome components in adipocytes, which indicated that Hcy acts as both the first and second signal activators of NLRP3 inflammasomes in adipocytes. As plasma levels of Hcy are increased

during obesity [26,64,65], Hcy could be one of the mediators, involved in the obesity-induced insulin resistance. Consistent with the present study, activation of the NLRP3 inflammasome was also found in the Hcy-induced abdominal aortic aneurysm, atherosclerosis and glomerular damage [33,66,67].

Saturated FA, ceramide, cardiolipin and lyso-PC, have been reported to act as second signal activators of the NLRP3 inflammasome [17,18,51,52,68]. In this study, lyso-PC was found to activate both adipocyte and ATM NLRP3 inflammasomes in autocrine and paracrine manners. Lyso-PC directly impaired insulin signaling [69]. Additionally, lyso-PC also acts as a lipid mediator in response to inflammation [70] and has been reported to exert a pro-inflammatory effect through modulating the chemotaxis and M1 polarization of macrophages [71,72]. Therefore, Hcy-induced adipocyte lyso-PC generation may also facilitate the infiltration, retention and activation of ATM. However, another study reported that lyso-PC improves insulin resistance and adipose inflammation through activating M2 polarization of ATMs [73]. Different functions of lyso-PC depend primarily on the different degrees of saturation of the lyso-PC acyl chain. The lyso-PC (18:1)-induced IL1β secretion was much less than lyso-PC (18:0) [74]. The saturated acyl lyso-PC was reported to strongly promote inflammation [75], while the polyunsaturated acyl lyso-PC reverses the saturated acyl lyso-PC-induced inflammation [76]. In the present study, Hcy treatment primarily increased the generation of saturated acyl lyso-PC in adipocytes. Therefore, the contrasting effects of lyso-PC on insulin resistance and adipose inflammation may be due to the different species of lyso-PC.

Lyso-PC has been reported to mediate CASP1 activation in a ROS-dependent manner [77]. However, as Hcy also increases intracellular ROS generation within 0.5 h [31], lyso-PC activation of the NLRP3 inflammasome may not occur in a ROS-dependent manner. In support of this, the lyso-PC-induced glial cell inflammasome activation depends on lysosomes damage, Ca^{2+} influx and K^{+} efflux but not on intracellular ROS [51,78]. Extracellular lyso-PC was reported to activate G protein-coupled receptors (GPRs), GPR132 and GPR4 [79]. GPR132 participates in the lyso-PC-induced Ca^{2+} influx and immune cell inflammation [70,80], which may be involved in the lyso-PC-induced NLRP3 inflammasome activation.

PLA2G16 was firstly recognized as a type II tumor suppressor gene [81] and was subsequently identified as a PPARγ target gene and a Ca^{2+}-independent PLA2, expressed specifically in adipose tissue [82,83]. Knockout of *Pla2g16* induces insulin resistance in mice [84], which appears inconsistent with the present results. The Land's cycle also remodels the saturation and mobility of membrane [85]. The complete loss of the basal level of PLA2G16 may block the remodeling of the membrane in hypertrophic adipocytes, inducing a phenotype of lipodystrophy in *Pla2g16* knockout mice [84].

HIF is a transcription factor that is stabilized and becomes transcriptionally active under hypoxia. Under normoxic conditions, HIFα is constitutively degraded by proteasomes; under hypoxic conditions, HIFα is stabilized and forms a heterodimer with HIFβ, regulating target gene expression [86]. With obesity, adipose HIF1 is activated due to adipose hypertrophy-induced hypoxia. Adipocyte HIF1 was reported to promote obesity, insulin resistance, adipose inflammation and fibrosis [87–90]. HIF1 was also been reported to activate inflammasomes by up-regulating IL1β expression [91]. In this study, activation of the adipose HIF1 was observed in Hcy-treated mice. The Hcy-induced insulin résistance and adipose inflammation were improved in the *Hif1a*$^{\Delta Ad}$ mice, which indicates a mechanism for Hcy-induced insulin resistance. *Pla2g16* was identified as a target gene of HIF1, which yields a mechanism for HIF1-induced adipose dysfunction.

In summary, this study demonstrates that the NLRP3 inflammasomes are activated in both adipocytes and ATMs, mediating the Hcy-induced insulin resistance. Hcy acts as a second signal activator of the adipocyte NLRP3 inflammasomes in a lyso-PC-dependent manner through adipocyte HIF1-PLA2G16 axis. Adipocyte-derived lyso-PC induces ATM inflammasome activation in a paracrine manner (Fig. 7g). The present study reveals the central role of the adipocyte in Hcy-induced adipose inflammasome activation and highlights the metabolic mechanisms, linking the initial stimulus for adipose dysfunction with insulin resistance.

Funding Sources

This work was supported by the National Natural Science Foundation of China (No. 91439206, 91739303, 81470554 and 81522007), the National Key Research and Development Program of China (No. 2016YFC0903100), China Postdoctoral Science Foundation (No. 2017M610717) and Special Program of Peking University for Clinical Medicine + X (No. PKU2017LCX09). S.Y. Zhang was supported in part by the Postdoctoral Fellowship of Peking-Tsinghua Center for Life Sciences. Funders had no role in study design, data interpretation and writing of the manuscript.

Conflicts of Interest

The authors declare no competing financial interest.

Author Contributions

S.Y.Z. and Y.Q.D. designed, performed, analyzed and interpreted the majority of animal and biochemical experiments, and drafted the manuscript; P.W., X.Z., Y.Y., L.S. and B.L. supported the animal experiments; D.Z. and H.Z. collected the clinical samples; H.L. performed and analyzed the lipidomics analysis; W.K., G.H., Y.M.S. and F.J.G. provided reagents and edited the manuscript; X.W. and C.J. designed, planned and interpreted the study and wrote the manuscript. S.Y.Z. and Y.Q.D. contributed equally to this work.

Appendix A. Supplementary Data

Supplementary data to this article can be found online at https://doi.org/10.1016/j.ebiom.2018.04.022.

References

Fain, J.N., Madan, A.K., Hiler, M.L., Cheema, P., Bahouth, S.W., 2004. Comparison of the release of adipokines by adipose tissue, adipose tissue matrix, and adipocytes from visceral and subcutaneous abdominal adipose tissues of obese humans. Endocrinology 145, 2273–2282.

Hotamisligil, G.S., Shargill, N.S., Spiegelman, B.M., 1993. Adipose expression of tumor necrosis factor-alpha: Direct role in obesity-linked insulin resistance. Science 259, 87–91.

Cho, K.W., Morris, D.L., Delproposto, J.L., Geletka, L., Zamarron, B., Martinez-Santibanez, G., et al., 2014. An MHC II-dependent activation loop between adipose tissue macrophages and CD4+ T cells controls obesity-induced inflammation. Cell Rep 9, 605–617.

Deng, T., Lyon, C.J., Minze, L.J., Lin, J., Zou, J., Liu, J.Z., et al., 2013. Class II major histocompatibility complex plays an essential role in obesity-induced adipose inflammation. Cell Metab 17, 411–422.

Thomou, T., Mori, M.A., Dreyfuss, J.M., Konishi, M., Sakaguchi, M., Wolfrum, C., et al., 2017. Adipose-derived circulating miRNAs regulate gene expression in other tissues. Nature 542, 450–455.

Ying, W., Riopel, M., Bandyopadhyay, G., Dong, Y., Birmingham, A., Seo, J.B., et al., 2017. Adipose tissue macrophage-derived exosomal miRNAs can modulate in vivo and in vitro insulin sensitivity. Cell 171, 372–384 [e12].

Schaffler, A., Scholmerich, J., 2010. Innate immunity and adipose tissue biology. Trends Immunol 31, 228–235.

Zhou, L., Cao, X., Fang, J., Li, Y., Fan, M., 2015. Macrophages polarization is mediated by the combination of PRR ligands and distinct inflammatory cytokines. Int J Clin Exp Pathol 8, 10964–10974.

Schroder, K., Tschopp, J., 2010. The inflammasomes. Cell 140, 821–832.

de Zoete, M.R., Palm, N.W., Zhu, S., Flavell, R.A., 2014. Inflammasomes. Cold Spring Harb Perspect Biol 6, a016287.

Man, S.M., Karki, R., Kanneganti, T.D., 2017. Molecular mechanisms and functions of pyroptosis, inflammatory caspases and inflammasomes in infectious diseases. Immunol Rev 277, 61–75.

Yang, C.A., Chiang, B.L., 2015. Inflammasomes and human autoimmunity: A comprehensive review. J Autoimmun 61, 1–8.

Li, X., Deroide, N., Mallat, Z., 2014. The role of the inflammasome in cardiovascular diseases. J Mol Med (Berl) 92, 307–319.

Skeldon, A.M., Faraj, M., Saleh, M., 2014. Caspases and inflammasomes in metabolic inflammation. Immunol Cell Biol 92, 304–313.

Stienstra, R., Joosten, L.A., Koenen, T., van Tits, B., van Diepen, J.A., van den Berg, S.A., et al., 2010. The inflammasome-mediated caspase-1 activation controls adipocyte differentiation and insulin sensitivity. Cell Metab 12, 593–605.

Stienstra, R., van Diepen, J.A., Tack, C.J., Zaki, M.H., van de Veerdonk, F.L., Perera, D., et al., 2011. Inflammasome is a central player in the induction of obesity and insulin resistance. Proc Natl Acad Sci U S A 108, 15324–15329.

Vandanmagsar, B., Youm, Y.H., Ravussin, A., Galgani, J.E., Stadler, K., Mynatt, R.L., et al., 2011. The NLRP3 inflammasome instigates obesity-induced inflammation and insulin resistance. Nat Med 17, 179–188.

Wen, H., Gris, D., Lei, Y., Jha, S., Zhang, L., Huang, M.T., et al., 2011. Fatty acid-induced NLRP3-ASC inflammasome activation interferes with insulin signaling. Nat Immunol 12, 408–415.

Sun, S., Xia, S., Ji, Y., Kersten, S., Qi, L., 2012. The ATP-P2X7 signaling axis is dispensable for obesity-associated inflammasome activation in adipose tissue. Diabetes 61, 1471–1478.

Yin, Z., Deng, T., Peterson, L.E., Yu, R., Lin, J., Hamilton, D.J., et al., 2014. Transcriptome analysis of human adipocytes implicates the NOD-like receptor pathway in obesity-induced adipose inflammation. Mol Cell Endocrinol 394, 80–87.

Clarke, R., Daly, L., Robinson, K., Naughten, E., Cahalane, S., Fowler, B., et al., 1991. Hyperhomocysteinemia: An independent risk factor for vascular disease. N Engl J Med 324, 1149–1155.

Fu, Y., Wang, X., Kong, W., 2017. Hyperhomocysteinaemia and vascular injury: Advances in mechanisms and drug targets. Br J Pharmacol 175, 1173–1189.

Mccully, K.S., 2015. Homocysteine and the pathogenesis of atherosclerosis. Expert Rev Clin Pharmacol 8, 211–219.

Ala, O.A., Akintunde, A.A., Ikem, R.T., Kolawole, B.A., Ala, O.O., Adedeji, T.A., 2017. Association between insulin resistance and total plasma homocysteine levels in type 2 diabetes mellitus patients in south west Nigeria. Diabetes Metab Syndr 11, S803–S809.

Meigs, J.B., Jacques, P.F., Selhub, J., Singer, D.E., Nathan, D.M., Rifai, N., et al., 2001. Fasting plasma homocysteine levels in the insulin resistance syndrome: The Framingham offspring study. Diabetes Care 24, 1403–1410.

Vaya, A., Rivera, L., Hernandez-Mijares, A., de la Fuente, M., Sola, E., Romagnoli, M., et al., 2012. Homocysteine levels in morbidly obese patients: Its association with waist circumference and insulin resistance. Clin Hemorheol Microcirc 52, 49–56.

Chen, A.R., Zhang, H.G., Wang, Z.P., Fu, S.J., Yang, P.Q., Ren, J.G., et al., 2010. C-reactive protein, vitamin B12 and C677T polymorphism of N-5,10-methylenetetrahydrofolate reductase gene are related to insulin resistance and risk factors for metabolic syndrome in Chinese population. Clin Invest Med 33, E290–7.

Kheradmand, M., Maghbooli, Z., Salemi, S., Sanjari, M., 2017. Associations of MTHFR C677T polymorphism with insulin resistance, results of NURSE Study (Nursing Unacquainted Related Stress Etiologies). J Diabetes Metab Disord 16, 22.

Dehkordi, E.H., Sedehi, M., Shahraki, Z.G., Najafi, R., 2016. Effect of folic acid on homocysteine and insulin resistance of overweight and obese children and adolescents. Adv Biomed Res 5, 88.

Dai, J., Li, W., Chang, L., Zhang, Z., Tang, C., Wang, N., et al., 2006. Role of redox factor-1 in hyperhomocysteinemia-accelerated atherosclerosis. Free Radic Biol Med 41, 1566–1577.

Li, Y., Jiang, C., Xu, G., Wang, N., Zhu, Y., Tang, C., et al., 2008. Homocysteine upregulates resistin production from adipocytes in vivo and in vitro. Diabetes 57, 817–827.

Li, Y., Zhang, H., Jiang, C., Xu, M., Pang, Y., Feng, J., et al., 2013. Hyperhomocysteinemia promotes insulin resistance by inducing endoplasmic reticulum stress in adipose tissue. J Biol Chem 288, 9583–9592.

Sun, W., Pang, Y., Liu, Z., Sun, L., Liu, B., Xu, M., et al., 2015. Macrophage inflammasome mediates hyperhomocysteinemia-aggravated abdominal aortic aneurysm. J Mol Cell Cardiol 81, 96–106.

Zhang, S.Y., Lv, Y., Zhang, H., Gao, S., Wang, T., Feng, J., et al., 2016. Adrenomedullin 2 improves early obesity-induced adipose insulin resistance by inhibiting the class II MHC in adipocytes. Diabetes 65, 2342–2355.

Qiao, C., Zhang, L.X., Sun, X.Y., Ding, J.H., Lu, M., Hu, G., 2017. Caspase-1 deficiency alleviates dopaminergic neuronal death via inhibiting caspase-7/AIF pathway in MPTP/p mouse model of Parkinson's disease. Mol Neurobiol 54, 4292–4302.

Tomita, S., Ueno, M., Sakamoto, M., Kitahama, Y., Ueki, M., Maekawa, N., et al., 2003. Defective brain development in mice lacking the Hif-1alpha gene in neural cells. Mol Cell Biol 23, 6739–6749.

Kim, W.Y., Safran, M., Buckley, M.R., Ebert, B.L., Glickman, J., Bosenberg, M., et al., 2006. Failure to prolyl hydroxylate hypoxia-inducible factor alpha phenocopies VHL inactivation in vivo. EMBO J 25, 4650–4662.

Xue, X., Ramakrishnan, S., Anderson, E., Taylor, M., Zimmermann, E.M., Spence, J.R., et al., 2013. Endothelial PAS domain protein 1 activates the inflammatory response in the intestinal epithelium to promote colitis in mice. Gastroenterology 145, 831–841.

Eguchi, J., Wang, X., Yu, S., Kershaw, E.E., Chiu, P.C., Dushay, J., et al., 2011. Transcriptional control of adipose lipid handling by IRF4. Cell Metab 13, 249–259.

Cho, K.W., Morris, D.L., Lumeng, C.N., 2014. Flow cytometry analyses of adipose tissue macrophages. Methods Enzymol 537, 297–314.

Majka, S.M., Miller, H.L., Helm, K.M., Acosta, A.S., Childs, C.R., Kong, R., et al., 2014. Analysis and isolation of adipocytes by flow cytometry. Methods Enzymol 537, 281–296.

Jiang, C., Kim, J.H., Li, F., Qu, A., Gavrilova, O., Shah, Y.M., et al., 2013. Hypoxia-inducible factor 1alpha regulates a SOCS3-STAT3-adiponectin signal transduction pathway in adipocytes. J Biol Chem 288, 3844–3857.

Nielsen, R., Mandrup, S., 2014. Genome-wide profiling of transcription factor binding and epigenetic marks in adipocytes by ChIP-seq. Methods Enzymol 537, 261–279.

Jiang, C., Xie, C., Li, F., Zhang, L., Nichols, R.G., Krausz, K.W., et al., 2015. Intestinal farnesoid X receptor signaling promotes nonalcoholic fatty liver disease. J Clin Invest 125, 386–402.

Xia, J., Wishart, D.S., 2016. Using MetaboAnalyst 3.0 for Comprehensive Metabolomics Data Analysis. Curr Protoc Bioinformatics 55, 14 10 1–14 10 91.

Li, P., Allen, H., Banerjee, S., Franklin, S., Herzog, L., Johnston, C., et al., 1995. Mice deficient in IL-1 beta-converting enzyme are defective in production of mature IL-1 beta and resistant to endotoxic shock. Cell 80, 401–411.

Rowe, S.J., Allen, L., Ridger, V.C., Hellewell, P.G., Whyte, M.K., 2002. Caspase-1-deficient mice have delayed neutrophil apoptosis and a prolonged inflammatory response to lipopolysaccharide-induced acute lung injury. J Immunol 169, 6401–6407.

Lamkanfi, M., Mueller, J.L., Vitari, A.C., Misaghi, S., Fedorova, A., Deshayes, K., et al., 2009. Glyburide inhibits the Cryopyrin/Nalp3 inflammasome. J Cell Biol 187, 61–70.

Mariathasan, S., Weiss, D.S., Newton, K., Mcbride, J., O'rourke, K., Roose-Girma, M., et al., 2006. Cryopyrin activates the inflammasome in response to toxins and ATP. Nature 440, 228–232.

Martinon, F., Petrilli, V., Mayor, A., Tardivel, A., Tschopp, J., 2006. Gout-associated uric acid crystals activate the NALP3 inflammasome. Nature 440, 237–241.

Freeman, L., Guo, H., David, C.N., Brickey, W.J., Jha, S., Ting, J.P., 2017. NLR members NLRC4 and NLRP3 mediate sterile inflammasome activation in microglia and astrocytes. J Exp Med 214, 1351–1370.

Iyer, S.S., He, Q., Janczy, J.R., Elliott, E.I., Zhong, Z., Olivier, A.K., et al., 2013. Mitochondrial cardiolipin is required for Nlrp3 inflammasome activation. Immunity 39, 311–323.

Murakami, M., Taketomi, Y., Miki, Y., Sato, H., Hirabayashi, T., Yamamoto, K., 2011. Recent progress in phospholipase A(2) research: From cells to animals to humans. Prog Lipid Res 50, 152–192.

Duncan, R.E., Sarkadi-Nagy, E., Jaworski, K., Ahmadian, M., Sul, H.S., 2008. Identification and functional characterization of adipose-specific phospholipase A2 (AdPLA). J Biol Chem 283, 25428–25436.

Li, C., Xia, M., Abais, J.M., Liu, X., Li, N., Boini, K.M., et al., 2013. Protective role of growth hormone against hyperhomocysteinemia-induced glomerular injury. Naunyn Schmiedebergs Arch Pharmacol 386, 551–561.

Lee, K., Zhang, H., Qian, D.Z., Rey, S., Liu, J.O., Semenza, G.L., 2009. Acriflavine inhibits HIF-1 dimerization, tumor growth, and vascularization. Proc Natl Acad Sci U S A 106, 17910–17915.

Garlanda, C., Dinarello, C.A., Mantovani, A., 2013. The interleukin-1 family: Back to the future. Immunity 39, 1003–1018.

Ballak, D.B., Stienstra, R., Tack, C.J., Dinarello, C.A., Van Diepen, J.A., 2015. IL-1 family members in the pathogenesis and treatment of metabolic disease: Focus on adipose tissue inflammation and insulin resistance. Cytokine 75, 280–290.

Jager, J., Gremeaux, T., Cormont, M., Le Marchand-Brustel, Y., Tanti, J.F., 2007. Interleukin-1beta-induced insulin resistance in adipocytes through down-regulation of insulin receptor substrate-1 expression. Endocrinology 148, 241–251.

Koenen, T.B., Stienstra, R., Van Tits, L.J., de Graaf, J., Stalenhoef, A.F., Joosten, L.A., et al., 2011. Hyperglycemia activates caspase-1 and TXNIP-mediated IL-1beta transcription in human adipose tissue. Diabetes 60, 517–524.

Kotas, M.E., Jurczak, M.J., Annicelli, C., Gillum, M.P., Cline, G.W., Shulman, G.I., et al., 2013. Role of caspase-1 in regulation of triglyceride metabolism. Proc Natl Acad Sci U S A 110, 4810–4815.

Chalkiadaki, A., Guarente, L., 2012. High-fat diet triggers inflammation-induced cleavage of SIRT1 in adipose tissue to promote metabolic dysfunction. Cell Metab 16, 180–188.

Niu, Z., Shi, Q., Zhang, W., Shu, Y., Yang, N., Chen, B., et al., 2017. Caspase-1 cleaves PPARgamma for potentiating the pro-tumor action of TAMs. Nat Commun 8, 766.

da Silva, N.P., de Souza, F.I., Pendezza, A.I., Fonseca, F.L., Hix, S., Oliveira, A.C., et al., 2013. Homocysteine and cysteine levels in prepubertal children: Association with waist circumference and lipid profile. Nutrition 29, 166–171.

Das, M., Ghose, M., Borah, N.C., Choudhury, N., 2010. A community based study of the relationship between homocysteine and some of the life style factors. Indian J Clin Biochem 25, 295–301.

Wang, R., Wang, Y., Mu, N., Lou, X., Li, W., Chen, Y., et al., 2017. Activation of NLRP3 inflammasomes contributes to hyperhomocysteinemia-aggravated inflammation and atherosclerosis in apoE-deficient mice. Lab Invest 97, 922–934.

Zhang, C., Boini, K.M., Xia, M., Abais, J.M., Li, X., Liu, Q., et al., 2012. Activation of Nod-like receptor protein 3 inflammasomes turns on podocyte injury and glomerular sclerosis in hyperhomocysteinemia. Hypertension 60, 154–162.

Scholz, H., Eder, C., 2017. Lysophosphatidylcholine activates caspase-1 in microglia via a novel pathway involving two inflammasomes. J Neuroimmunol 310, 107–110.

Han, M.S., Lim, Y.M., Quan, W., Kim, J.R., Chung, K.W., Kang, M., et al., 2011. Lysophosphatidylcholine as an effector of fatty acid-induced insulin resistance. J Lipid Res 52, 1234–1246.

Kabarowski, J.H., 2009. G2A and LPC: Regulatory functions in immunity. Prostaglandins Other Lipid Mediat 89, 73–81.

Qin, X., Qiu, C., Zhao, L., 2014. Lysophosphatidylcholine perpetuates macrophage polarization toward classically activated phenotype in inflammation. Cell Immunol 289, 185–190.

Yang, L.V., Radu, C.G., Wang, L., Riedinger, M., Witte, O.N., 2005. Gi-independent macrophage chemotaxis to lysophosphatidylcholine via the immunoregulatory GPCR G2A. Blood 105, 1127–1134.

Zhu, X., Zong, G., Zhu, L., Jiang, Y., Ma, K., Zhang, H., et al., 2014. Deletion of class A scavenger receptor deteriorates obesity-induced insulin resistance in adipose tissue. Diabetes 63, 562–577.

Liu-Wu, Y., Hurt-Camejo, E., Wiklund, O., 1998. Lysophosphatidylcholine induces the production of IL-1beta by human monocytes. Atherosclerosis 137, 351–357.

Aiyar, N., Disa, J., Ao, Z., Ju, H., Nerurkar, S., Willette, R.N., et al., 2007. Lysophosphatidylcholine induces inflammatory activation of human coronary artery smooth muscle cells. Mol Cell Biochem 295, 113–120.

Hung, N.D., Sok, D.E., Kim, M.R., 2012. Prevention of 1-palmitoyl lysophosphatidylcholine-induced inflammation by polyunsaturated acyl lysophosphatidylcholine. Inflamm Res 61, 473–483.
Schilling, T., Eder, C., 2011. Sodium dependence of lysophosphatidylcholine-induced caspase-1 activity and reactive oxygen species generation. Immunobiology 216, 118–125.
Stock, C., Schilling, T., Schwab, A., Eder, C., 2006. Lysophosphatidylcholine stimulates IL-1beta release from microglia via a P2X7 receptor-independent mechanism. J Immunol 177, 8560–8568.
Meyer zu Heringdorf, D., Jakobs, K.H., 2007. Lysophospholipid receptors: Signalling, pharmacology and regulation by lysophospholipid metabolism. Biochim Biophys Acta 1768, 923–940.
Khan, S.Y., Mclaughlin, N.J., Kelher, M.R., Eckels, P., Gamboni-Robertson, F., Banerjee, A., et al., 2010. Lysophosphatidylcholines activate G2A inducing G(alphai)(−)(1)−/G(alphaq/)(1)(1)- Ca(2)(+) flux, G(betagamma)-Hck activation and clathrin/beta-arrestin-1/GRK6 recruitment in PMNs. Biochem J 432, 35–45.
Sers, C., Emmenegger, U., Husmann, K., Bucher, K., Andres, A.C., Schafer, R., 1997. Growth-inhibitory activity and downregulation of the class II tumor-suppressor gene H-rev107 in tumor cell lines and experimental tumors. J Cell Biol 136, 935–944.
Hummasti, S., Hong, C., Bensinger, S.J., Tontonoz, P., 2008. HRASLS3 is a PPARgamma-selective target gene that promotes adipocyte differentiation. J Lipid Res 49, 2535–2544.
Uyama, T., Morishita, J., Jin, X.H., Okamoto, Y., Tsuboi, K., Ueda, N., 2009. The tumor suppressor gene H-Rev107 functions as a novel Ca2+-independent cytosolic phospholipase A1/2 of the thiol hydrolase type. J Lipid Res 50, 685–693.
Jaworski, K., Ahmadian, M., Duncan, R.E., Sarkadi-Nagy, E., Varady, K.A., Hellerstein, M.K., et al., 2009. AdPLA ablation increases lipolysis and prevents obesity induced by high-fat feeding or leptin deficiency. Nat Med 15, 159–168.
Kazachkov, M., Chen, Q., Wang, L., Zou, J., 2008. Substrate preferences of a lysophosphatidylcholine acyltransferase highlight its role in phospholipid remodeling. Lipids 43, 895–902.
Taylor, C.T., Colgan, S.P., 2017. Regulation of immunity and inflammation by hypoxia in immunological niches. Nat Rev Immunol 17, 774–785.
Halberg, N., Khan, T., Trujillo, M.E., Wernstedt-Asterholm, I., Attie, A.D., Sherwani, S., et al., 2009. Hypoxia-inducible factor 1alpha induces fibrosis and insulin resistance in white adipose tissue. Mol. Cell Biol. 29, 4467–4483.
Jiang, C., Qu, A., Matsubara, T., Chanturiya, T., Jou, W., Gavrilova, O., et al., 2011. Disruption of hypoxia-inducible factor 1 in adipocytes improves insulin sensitivity and decreases adiposity in high-fat diet-fed mice. Diabetes 60, 2484–2495.
Lee, Y.S., Kim, J.W., Osborne, O., Oh, D.Y., Sasik, R., Schenk, S., et al., 2014. Increased adipocyte O2 consumption triggers HIF-1alpha, causing inflammation and insulin resistance in obesity. Cell 157, 1339–1352.
Zhang, X., Lam, K.S., Ye, H., Chung, S.K., Zhou, M., Wang, Y., et al., 2010. Adipose tissue-specific inhibition of hypoxia-inducible factor 1{alpha} induces obesity and glucose intolerance by impeding energy expenditure in mice. J Biol Chem 285, 32869–32877.
Zhang, W., Petrovic, J.M., Callaghan, D., Jones, A., Cui, H., Howlett, C., et al., 2006. Evidence that hypoxia-inducible factor-1 (HIF-1) mediates transcriptional activation of interleukin-1beta (IL-1beta) in astrocyte cultures. J Neuroimmunol 174, 63–73.